1.0

1.1

1.25   1.4   1.6

4.5
5.0
5.6
6.3
7.1

2.8   2.5
3.2   2.2
3.6
4.0   2.0
1.8

MICROCOPY RESOLUTION TEST CHART
NATIONAL BUREAU OF STANDARDS-1963-A

AMRL-TR-79-29

LEVEL

OPTICAL POWER SPECTRUM ANALYSIS OF PROCESSED IMAGERY

RICHARD A. SCHINDLER
BOEING AEROSPACE COMPANY
NAVY SYSTEMS AND ADVANCED PROJECTS DIVISION
SEATTLE, WASHINGTON 98124

JULY 1979

D D C
RECEIVED
AUG 23 1979
C

Approved for public release; distribution unlimited.

AEROSPACE MEDICAL RESEARCH LABORATORY
AEROSPACE MEDICAL DIVISION
AIR FORCE SYSTEMS COMMAND
WRIGHT-PATTERSON AIR FORCE BASE, OHIO 45433

79 08 23 087

NOTICES

Please do not request copies of this report from Aerospace Medical Research Laboratory. Additional copies may be purchased from:

> National Technical Information Service
> 5285 Port Royal Road
> Springfield, Virginia 22161

Federal Government agencies and their contractors registered with Defense Documentation Center should direct requests for copies of this report to:

> Defense Documentation Center
> Cameron Station
> Alexandria, Virginia 22314

TECHNICAL REVIEW AND APPROVAL

AMRL-TR-79-29

This report has been reviewed by the Information Office (OI) and is releasable to the National Technical Information Service (NTIS). At NTIS, it will be available to the general public, including foreign nations.

This technical report has been reviewed and is approved for publication.

FOR THE COMMANDER

CHARLES BATES, JR.
Chief
Human Engineering Division
Aerospace Medical Research Laboratory

(19) REPORT DOCUMENTATION PAGE		READ INSTRUCTIONS BEFORE COMPLETING FORM
(18) 1. REPORT NUMBER AMRL-TR-79-29	2. GOVT ACCESSION NO.	3. RECIPIENT'S CATALOG NUMBER
(6) 4. TITLE *(and Subtitle)* OPTICAL POWER SPECTRUM ANALYSIS OF PROCESSED IMAGERY.	(9)	5. TYPE OF REPORT & PERIOD COVERED Final report. 10 Jan 1978 - 30 June 1979 6. PERFORMING ORG. REPORT NUMBER
(10) 7. AUTHOR(s) Richard A. /Schindler	(15)	8. CONTRACT OR GRANT NUMBER(s) F33615-78-C-0503
9. PERFORMING ORGANIZATION NAME AND ADDRESS Boeing Aerospace Company Navy Systems and Advanced Projects Seattle, Washington 98124		10. PROGRAM ELEMENT, PROJECT, TASK AREA & WORK UNIT NUMBERS (16) 61102F, 2313-V1-24 (17) V1
11. CONTROLLING OFFICE NAME AND ADDRESS Aerospace Medical Research Lab., Aerospace Medical Division, Air Force Systems Command, Wright-Patterson Air Force Base, Ohio 45433		(11) 12. REPORT DATE July 1979 13. NUMBER OF PAGES 80
14. MONITORING AGENCY NAME & ADDRESS*(if different from Controlling Office)* (12) 80p.		15. SECURITY CLASS. *(of this report)* Unclassified 15a. DECLASSIFICATION/DOWNGRADING SCHEDULE

16. DISTRIBUTION STATEMENT *(of this Report)*

Approved for public release; distribution unlimited

17. DISTRIBUTION STATEMENT *(of the abstract entered in Block 20, if different from Report)*

18. SUPPLEMENTARY NOTES

19. KEY WORDS *(Continue on reverse side if necessary and identify by block number)*
Diffraction Pattern Sampling
Digital Image Processing
Information Theory
Optical Power Spectrum
Observer Target Recognition

20. ABSTRACT *(Continue on reverse side if necessary and identify by block number)*

This report describes the approach, procedures and results of a study to examine the use of information density values based on image power spectra as tools in the selection and application of digital image processing techniques. Information density measures are determined for unprocessed and processed imagery and compared with observer target recognition performance. The report describes modifications to the information density measure to improve the relationship with performance and to select the most effective processing technique.

DD FORM
1 JAN 73 **1473** EDITION OF 1 NOV 65 IS OBSOLETE

SUMMARY

PURPOSE

The ultimate goal of the work reported here is the development of a systematic, quantitative approach for the application of digital image processing techniques. The specific objective in this study is to examine the use of power spectrum sampling and information theory metrics as potential tools for such an application.

APPROACH

A series of images of tactical military vehicles mounted on a terrain table was acquired, digitized and computer processed with four processing techniques selected as representative of current digital processing. The results along with the original (base-line) imagery were printed with a laser beam recorder. Optical power spectrum sampling was used to obtain image measurements for the appropriate calculations of information density which were then compared with the results of observer target recognition performance using the base-line and processed imagery. The use of the information density values as a tool for selecting the most effective processing technique was assessed.

Processing techniques used in the study were:

- histogram equalization

- just noticable difference normalization

- linear frequency filtering

- logarithmic frequency filtering

Image variables were:

- target reflectance level

- scale/ground sampled distance

RESULTS AND CONCLUSIONS

It is important to note that this study is not intended as a definitive evaluation of the image processing techniques employed here. The test conditions are much too restrictive to permit broad generalizations about the

overall effectiveness of any of the image processing techniques.

Under the conditions tested here:

1) The histogram modification techniques (histogram equalization and J.N.D. normalization) were the most successful, particularly with low contrast imagery.

2) All processing techniques performed poorly with high reflectance targets, probably because of saturation with the contrast stretching.

3) Both frequency filtering techniques performed poorly although the "homomorphic" (logarithmic) technique was clearly superior to the linear model.

4) The "pure" theoretical information density measure is not effective as a measure of processing effects on observer performance (r = -.33).

5. Corrections for visual sine-wave thresholds and for overall image contrast greatly improve the information density relationships with performance (r = .95).

6. A process selection technique based on modified information density measures of the original (base-line) image is a feasible alternative to the "try and see" approach to digital image processing. Measures calculated directly from the original digital image data may also be used for this purpose.

PREFACE

This report was prepared by the Advanced Requirements organization, Naval Systems and Advanced Projects Division of the Boeing Aerospace Company, Seattle Washington. The work was done under USAF Contract F33615-78-C-0503, for the Visual Display Systems Branch, Human Engineering Division, of the Aerospace Medical Research Laboratory. Mr. Wayne Martin was the Technical Monitor for the Air Force.

The contract effort was initiated in January 1978 and completed in June 1979. Mr. J. Booth was Program Manager and Mr. R. Schindler was Principal Investigator for The Boeing Company.

Significant contributions to the research effort were made by Mr. C. Pyle for observer performance data collection, Mr. R. Turner and Dr. C. Allen for digital image processing and Mr. B. Wittman and Mr. E. Jones for display systems laboratory support.

TABLE OF CONTENTS

4

SECTION I

INTRODUCTION

This study is an extension of previous work reported by Schindler and Martin (1978). The initial effort was concerned with the use of optical power spectrum (OPS) sampling to determine information density measures for CRT imagery. The effectiveness of this measurement technique was evaluated through observer performance testing under a variety of CRT operating conditions. The results demonstrated good relationships between the information density measures and CRT levels of dynamic range and bandwidth and between information density and observer performance.

The present study is concerned with application of optical power sampling and information theory to the evaluation of digital hardcopy imagery (positive transparencies) including the use of some representative digital image processing techniques (histogram modification and spatial filtering). It is important to note that the primary objective of this study is not to evaluate the general effectiveness of digital data processing techniques, but rather to examine the information density measure as an evaluation tool. The processing techniques used were selected and implemented as typical approaches to digital data processing and used as vehicles for evaluation of the information density measure. They are not intended to represent optimum digital processing techniques. Experience with a variety of image processing techniques indicates that no single procedure is universally effective. The improvement effected by most techniques is largely dependent on the characteristics of the original imagery. Clearly, if the original image is of sufficient quality to provide maximum perceptability of the desired information, additional processing will be of little value. Conversely, if the desired information does not exist in the original image data, processing may still not provide a solution.

The basic goal of this effort is to apply OPS and information density metrics to the evaluation of a representative sample of state-of-the-art image processing algorithms and relate these metrics to observer performance. The

5

resulting relationships will, hopefully, be useful to guide the develop-
ment of rapid selection techniques for alternate candidate image process-
ing algorithms. In addition, the results of this effort should assist in
the specification of advanced experimental algorithms for which no object-
ive human performance data exists. It is intended that information gleaned
from this effort will provide a more systematic approach to the selection
and implementation of image processing techniques than is currently avail-
able.

The following sections in this report provide background information sum-
marizing the processing algorithms used here and describe the OPS samp-
ling technique and application of information theory for determining image
information density values. This is followed by a description of the approach,
procedures and results of this study effort including stimulus image genera-
tion and observer performance testing. Evaluations of the results and dis-
cussions of potential applications are included.

SECTION II

BACKGROUND

DIGITAL IMAGE PROCESSING

A digitized image is the result of a sampling process that produces an array of numbers describing the image luminance level at each point in the array. The individual points are generally called elements or pixels. The individual numbers are frequently quantized, i.e., assigned one of a set of discrete values. An important property of such digitization is the ease with which such numerical arrays can be manipulated by computers. This property has led to the development of a wide variety of processing algorithms intended to improve the efficiency and/or effectiveness of the digital image array. Three major areas of application are involved:

1) Coding - The objective of these techniques is to improve the efficiency of the image data package so as to reduce storage and/or transmission requirements.

2) Enhancement - These techniques are intended to improve the perceptability of relevant information in the image and/or to improve the general "appearance" of the image.

3) Automatic Recognition - These approaches are concerned with the classification or description of images or image parts on the basis of measurable numerical properties or characteristics of the image arrays.

Good reviews of algorithms developed in all three areas are provided in books by Rosenfeld and Kak (1976) and by Gonzalez and Wintz (1977). An excellent bibliography on earlier literature in the area has been prepared by the University of Southern California (1972). Additional reviews are available by Hunt (1976) and Andrews (1976).

Very few studies in the literature involve systematic evaluations of processing effectiveness. Most efforts present theoretical developments of processing techniques and the inclusion of selected examples of the effects.

7

Some notable exceptions to the above include Mannos and Sakrison (1974), Agrawal and O'Neal (1973), and Ketcham, et. al. (1976). The above studies use image quality judgments as evaluation criteria. Studies using measures of information extraction performance as evaluation criteria are much less common. These include Humes and Bauerschmidt (1968) and Gaven, et. al. (1970).

All of the processing techniques considered in this study are limited to the second area, enhancement. Five major classes of algorithms are commonly used in the enhancement area.

1) Grey-level or histogram modification - This class of algorithms reassigns individual luminance values within the image array to achieve or approach some desired frequency distribution of luminance levels.

2) Spatial-frequency filtering - These algorithms are designed to modify the image content as a function of spatial frequency. Such algorithms can, for example, be used to highlight the very fine detail in an image by enhancing the high frequency content.

3) Sharpening - So-called edge enhancement techniques are concerned with increasing the contrast and/or sharpness of edges in the image. Although this effect can be achieved with frequency filtering, algorithms exist for performing this operation in the spatial domain.

4) Smoothing - This class is essentially the complement of the sharpening techniques. Smoothing algorithms are designed to eliminate unwanted discontinuities or variations in the image such as noise or scan lines.

5) Geometric corrections - Geometric distortions because of scanning operations or acquisition geometry can be minimized or eliminated by computer-controlled repositioning of individual image elements. These corrections can be especially important for mapping applications or stereoscopic viewing of the imagery.

8

Techniques selected for consideration in this study are limited to the
first two classes, histogram modification and spatial frequency filter-
ing.

HISTOGRAM MODIFICATION

The frequency distribution of luminance or grey level values in an image
is called the image histogram. Figure 1 presents an example for one of
the images used in this study. The distribution indicates that the grey
levels are shifted toward the dark end of the scale and occupy only about
two-thirds of the available range of 256 levels (8 bits). Algorithms exist
for re-assigning grey level values to produce a revised histogram that
approximates any desired distribution. A detailed description of this
process is presented in most reference books on image processing. See,
for example, Pratt (1978).

A very common procedure is to produce a histogram that fills the avail-
able range and at the same time provides a nearly flat frequency distri-
bution. Figure 2 illustrates the application of this technique to the
example of Figure 1. The effects of this technique as cited by Rosenfeld
and Kak (1976) are to stretch the points in the densely populated regions
of the grey scale and to compress *the sparsely populated points*. The re-
sulting distribution has the property of representing the maximum informa-
tion content in the sense of formal information theory. This property is
especially relevant to the evaluation techniques considered in this study.
Additional discussions of the histogram normalization technique are pro-
vided by Hall (1974) and Andrews (1976).

The original histogram can be modified to approximate any desired distri-
bution, not just the flat distribution discussed above. Another promising
approach is to redistribute the grey levels into steps that approximate
the human visual sensitivity curve for discrimination of grey levels. The
specific algorithm used in this study, referred to as "just noticeable dif-
ference" (J.N.D.) equalization is based on an empirical model developed by
Rogers and Carel (1973). This transfer function, shown in Figure 3, com-
presses the dark end of the scale where visual discrimination is most

9

CANVAS TRUCK
0.8 FT. G.S.D.
33% REFLECTANCE

FREQUENCY

SIGNAL LEVEL
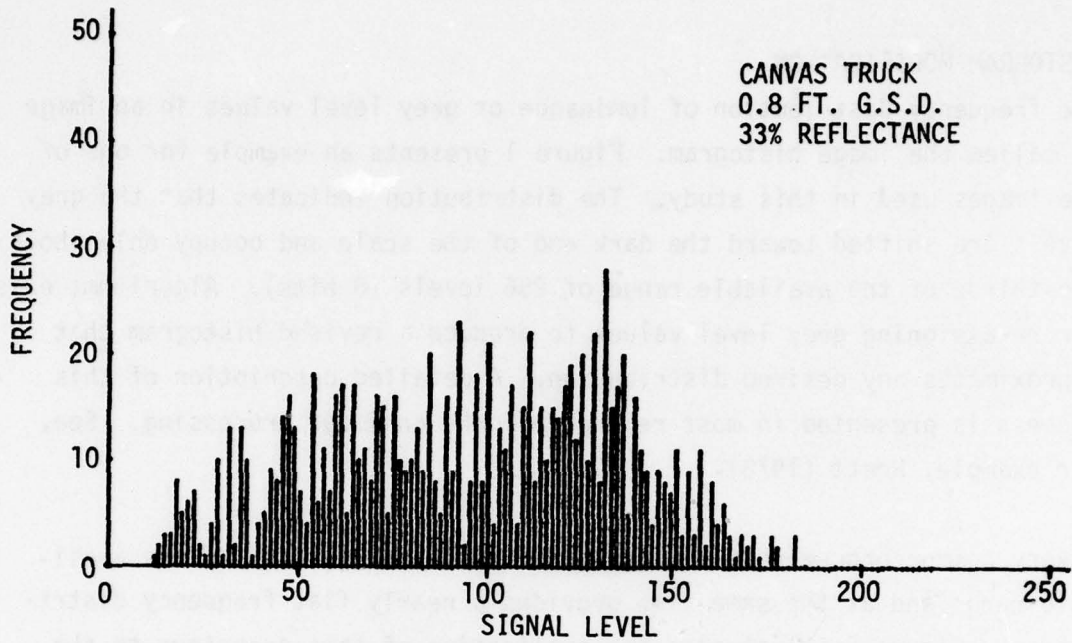
Figure 1: Histogram for non-processed image.

CANVAS TRUCK
0.8 FT. G.S.D.
33% REFLECTANCE

FREQUENCY

SIGNAL LEVEL
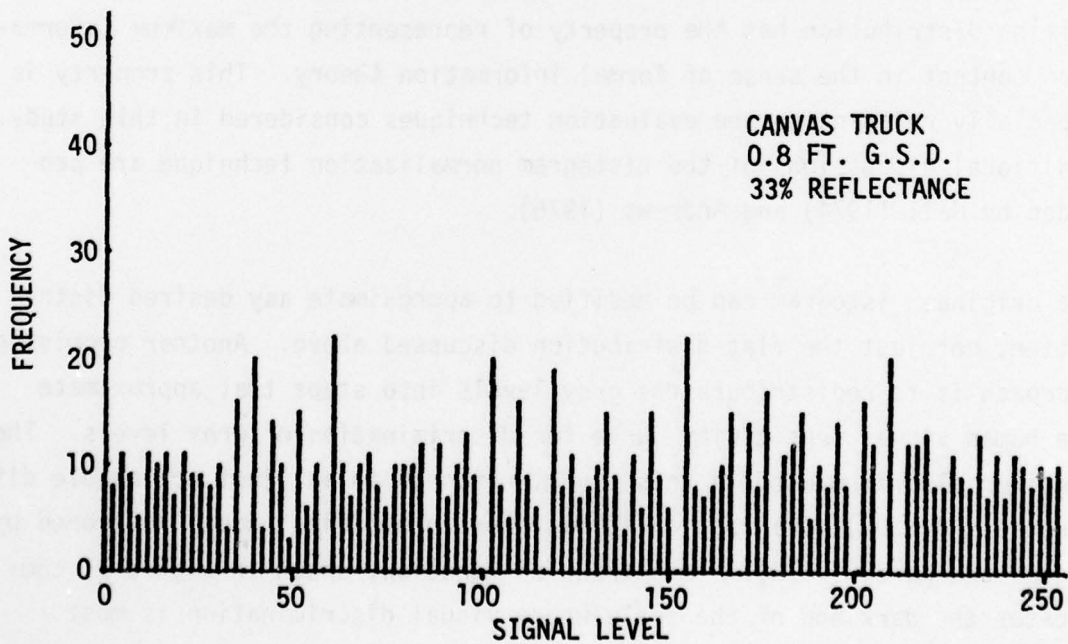
Figure 2: Histogram for above image after equalization.

10
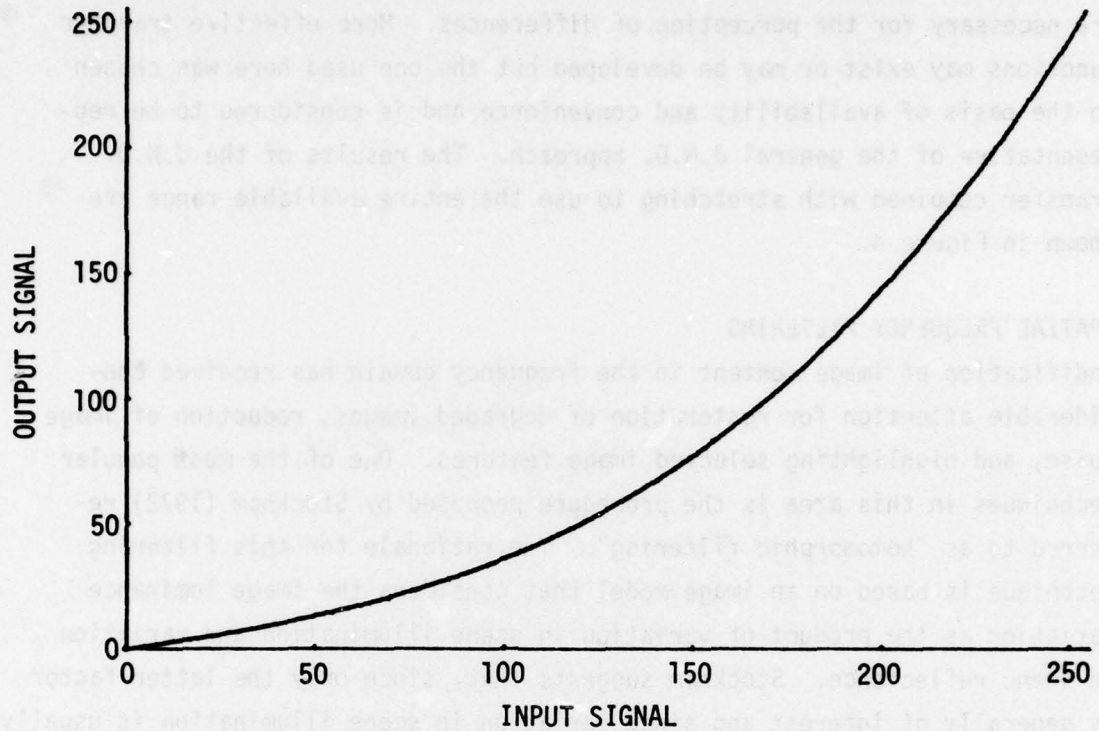
Figure 3: Transfer function used for J.N.D. equalization.

CANVAS TRUCK
0.8 FT. G.S.D.
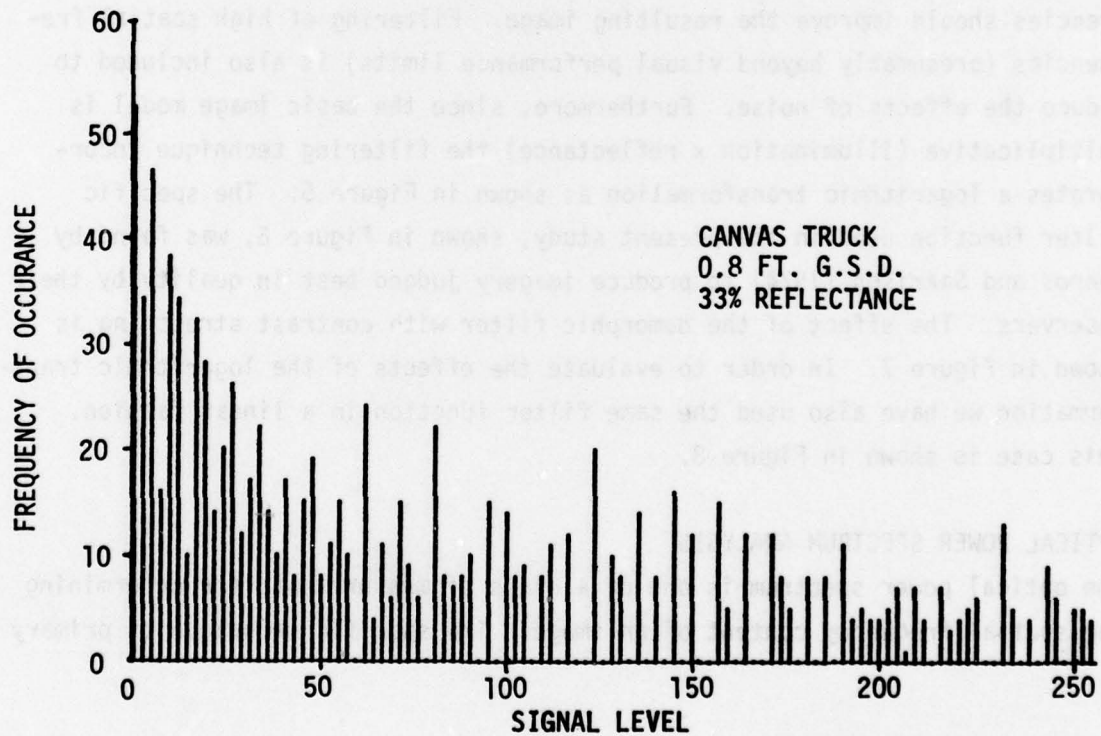33% REFLECTANCE

Figure 4: Histogram after J.N.D. equalization.

11

effective and expands the light end where larger luminance differences are necessary for the perception of differences. More effective transfer functions may exist or may be developed but the one used here was chosen on the basis of availability and convenience and is considered to be representative of the general J.N.D. approach. The results of the J.N.D. transfer combined with stretching to use the entire available range are shown in Figure 4.

SPATIAL FREQUENCY FILTERING

Modification of image content in the frequency domain has received considerable attention for restoration of degraded images, reduction of image noise, and highlighting selected image features. One of the most popular techniques in this area is the procedure proposed by Stockham (1972) referred to as "homomorphic filtering". The rationale for this filtering technique is based on an image model that considers the image luminance variation as the product of variation in scene illumination and variation in scene reflectance. Stockham suggests that, since only the latter factor is generally of interest and since variation in scene illumination is usually of very low spatial frequency, reducing the image content at these low frequencies should improve the resulting image. Filtering of high spatial frequencies (presumably beyond visual performance limits) is also included to reduce the effects of noise. Furthermore, since the basic image model is multiplicative (illumination x reflectance) the filtering technique incorporates a logarithmic transformation as shown in Figure 5. The specific filter function used in the present study, shown in Figure 6, was found by Mannos and Sakrison (1974) to produce imagery judged best in quality by their observers. The effect of the homorphic filter with contrast stretching is shown in Figure 7. In order to evaluate the effects of the logarithmic transformation we have also used the same filter function in a linear fashion. This case is shown in Figure 8.

OPTICAL POWER SPECTRUM ANALYSIS

The optical power spectrum is one of a class of measurements for determining the spatial frequency content of an image. The specific technique of primary

12

INPUT —— LOG —— FOURIER TRANSFORM —— FILTER H(k) —— INVERSE FOURIER TRANSFORM —— EXP —— OUTPUT
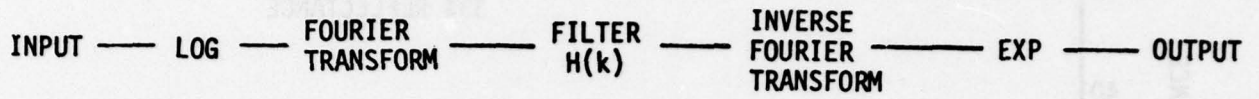
Figure 5: Homomorphic filtering prodedure.
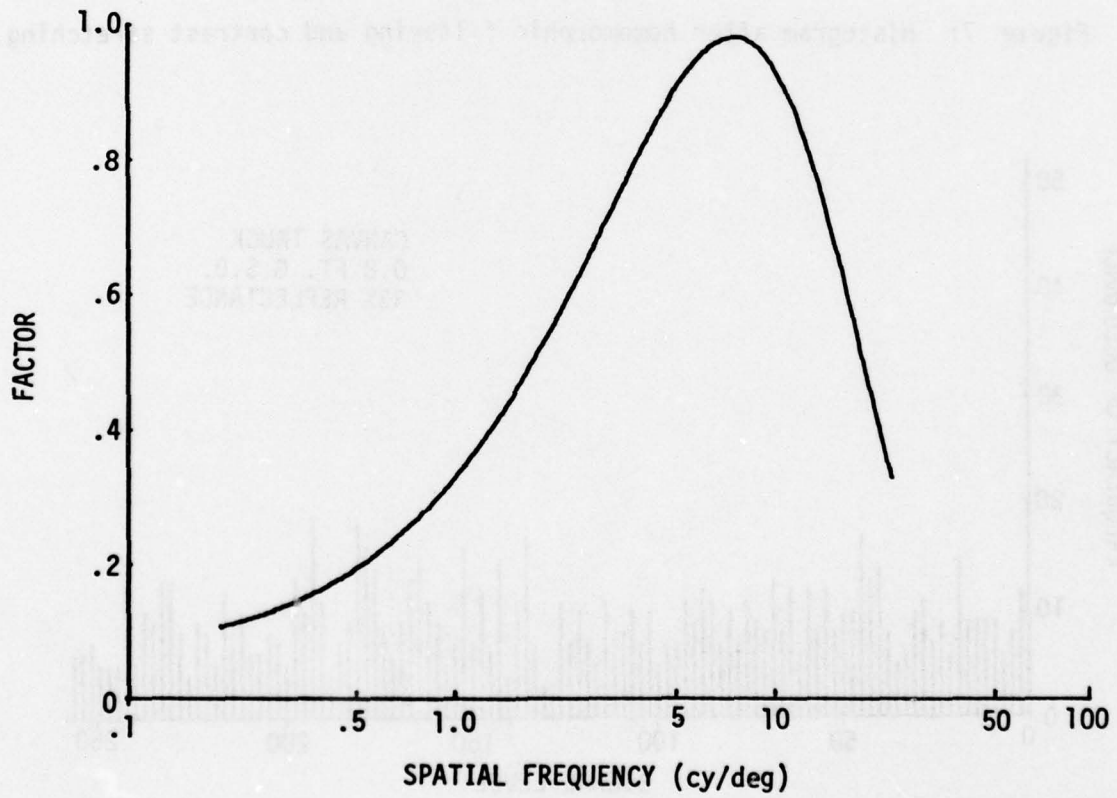
Figure 6: Spatial frequency filter function.

13

CANVAS TRUCK
0.8 FT. G.S.D.
33% REFLECTANCE
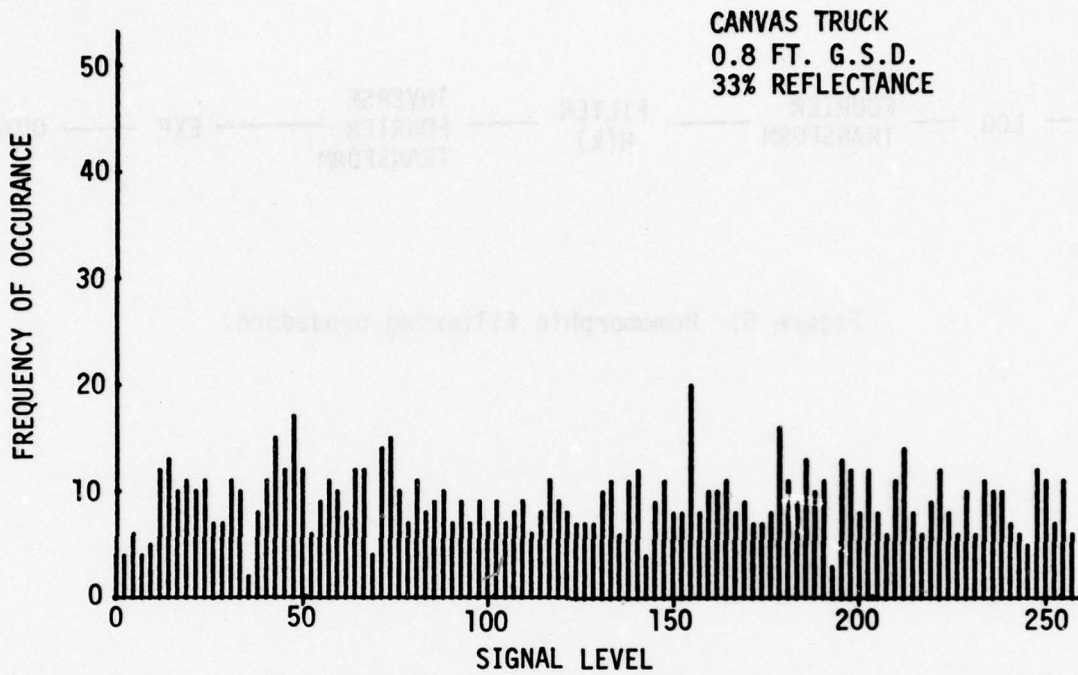
Figure 7: Histogram after homomorphic filtering and contrast stretching.
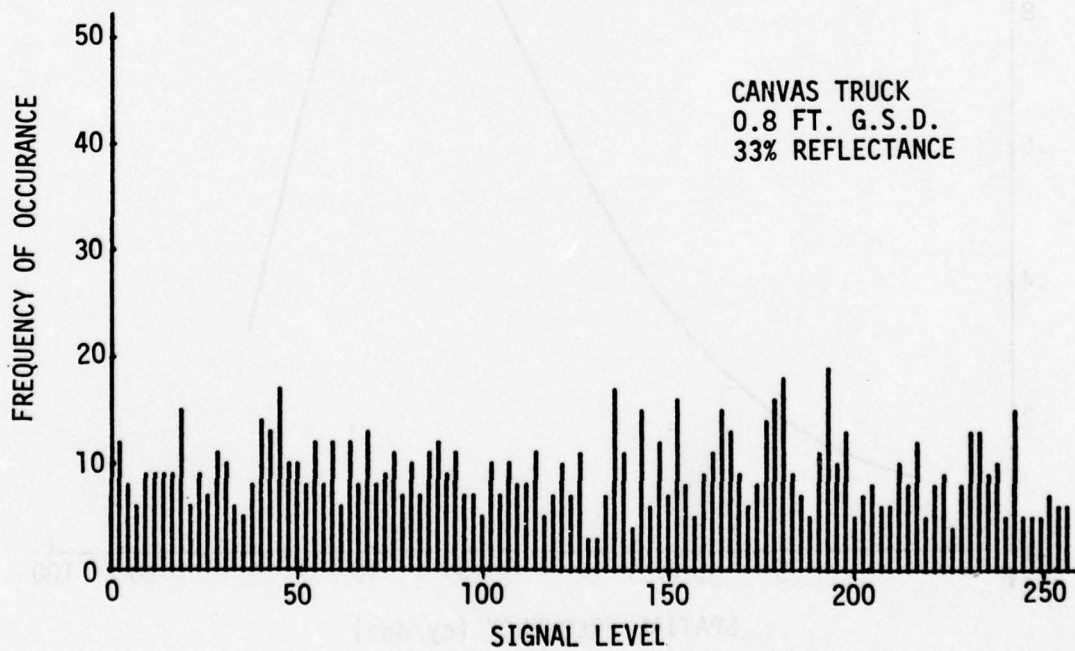
CANVAS TRUCK
0.8 FT. G.S.D.
33% REFLECTANCE

Figure 8: Histogram after linear spatial filtering and contrast stretching.

14

interest here uses an optical analog of the familiar Fourier transform
to translate image content from spatial dimensions (units of distance)
to frequency dimensions (units of cycles per distance). Similar results
can also be obtained, if the imagery has been digitized, by direct appli-
cation of the Fourier transform to the digital data.

Figure 9 presents a familiar example of a power spectrum; that for a
square wave grid pattern. This spectrum, as derived in most optics text-
books (see Goodman, 1968, for example), can be expressed as,

$$P(k) = \left(\frac{\sin(\pi Wk)}{\pi Wk} \right)^2 \left(\frac{\sin (N\pi Sk)}{\sin (\pi Sk)} \right)^2 \quad ,$$

where,

$P(k)$ = power at frequency k,
W = width of the clear spaces in the grid,
S = width of one cycle (bar + space) in the grid, and
N = the number of bars in the grid.

The plot on the left, in linear units, is the one most frequently presented.
Because of the very large dynamic range in power values, it is often more
informative to use the logarithmic plot shown on the right.

The spectrum can be interpreted as a descriptor of several properties of
the input grid image. For example, the largest "spike" in the spectrum is
located at the fundamental frequency of the grid (2 cycles per inch). The
spikes at the higher harmonics, located at multiples of the fundamental fre-
quency, are related to the bar-to-space width ratio and the number of bars.
In this theoretical example, the pattern modulation is 1.0 and the edges of
the bars are perfectly sharp. In any practical measurement, the spectrum is
also a function of the modulation and the sharpness of the grid bar edges.

The power spectrum has additional important and useful theoretical proper-
ties. The effect of a display with a known modulation transfer function,
for example, can be predicted as shown in Figure 10. The fall-off at high

15
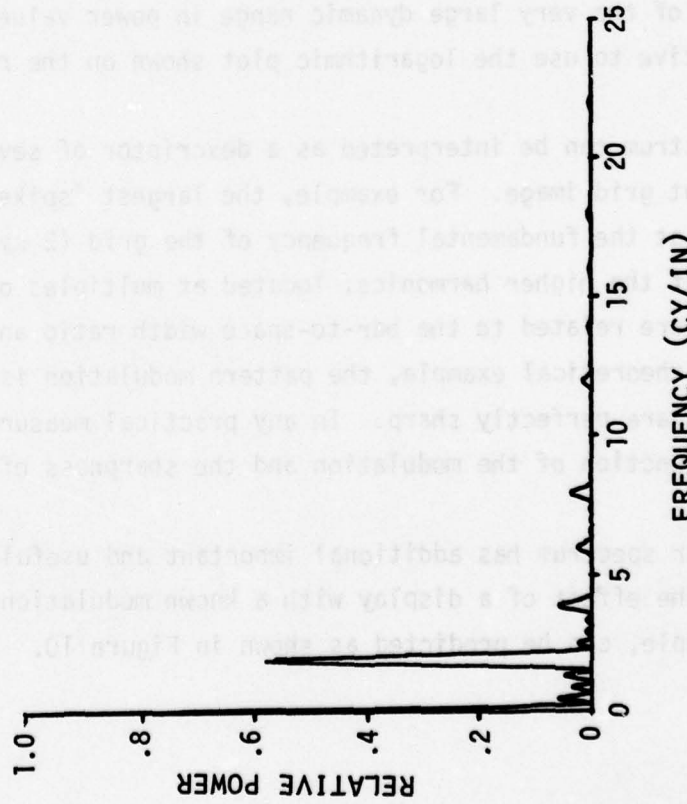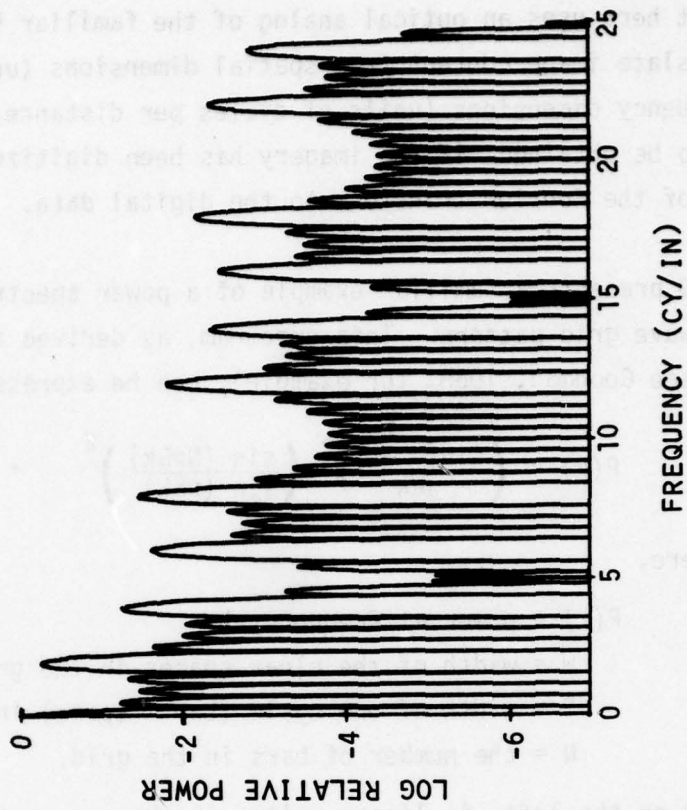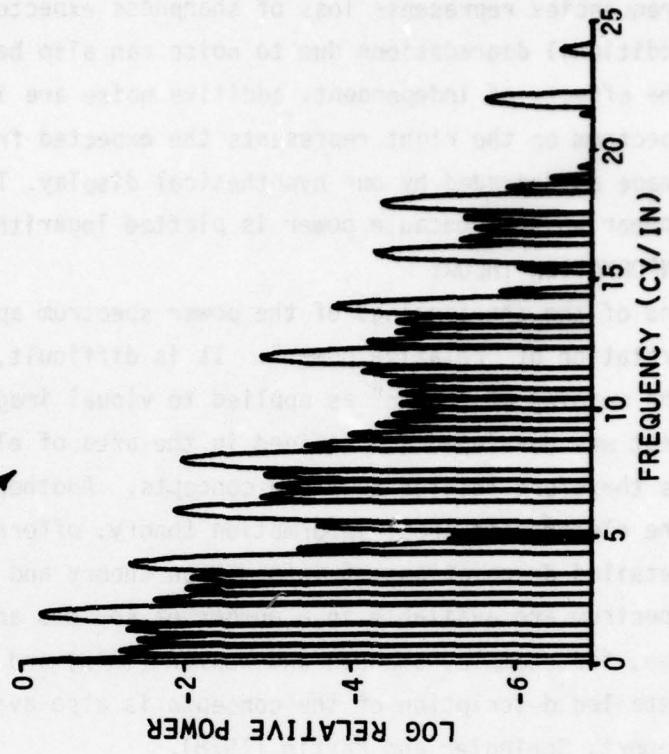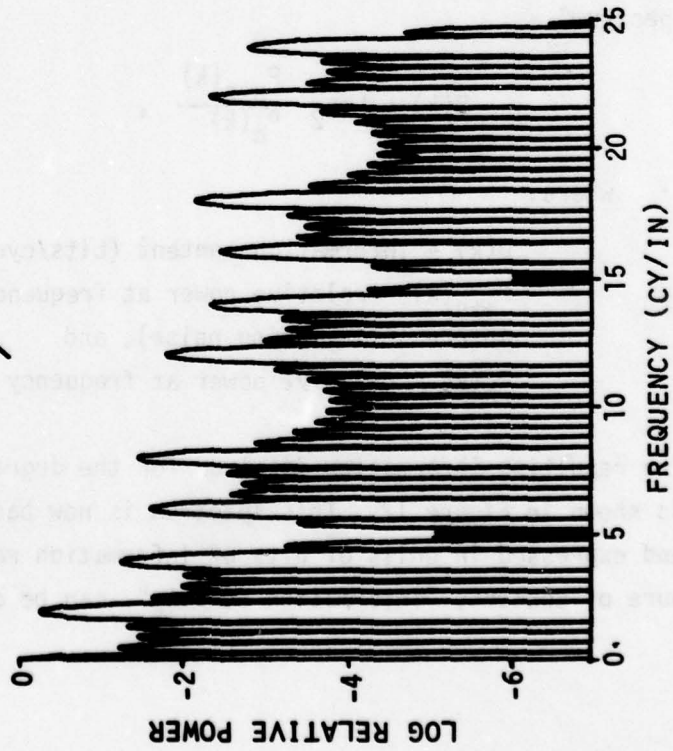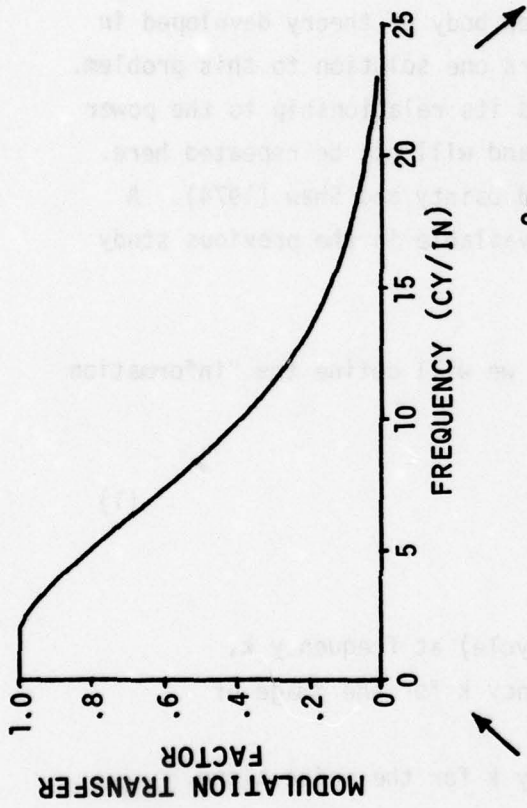
Figure 10: Effect of modulation transfer on the grid power spectrum.

FREQUENCY (CY/IN)

LOG RELATIVE POWER

MODULATION TRANSFER FACTOR

frequencies represents loss of sharpness expected in the displayed image. Additional degradations due to noise can also be predicted. In Figure 11, the effects of independent, additive noise are illustrated. The final spectrum on the right represents the expected frequency content of the grid image as degraded by our hypothetical display. The effects of additivity may appear unusual because power is plotted logarithmically.

INFORMATION THEORY

One of the shortcomings of the power spectrum approach lies in the interpretation of "relative power". It is difficult, intuitively, to understand the meaning of "power" as applied to visual imagery. The power spectrum concept was developed and refined in the area of electronics and the terminology is therefore related to those concepts. Another body of theory developed in the electronics area, information theory, offers one solution to this problem. Detailed descriptions of information theory and its relationship to the power spectrum are available in a number of sources and will not be repeated here. See, for example, Shannon and Weaver (1949) and Dainty and Shaw (1974). A detailed description of the concepts is also available in the previous study report, Schindler and Martin (1978).

Based on the principals of information theory, we will define the "information spectrum" as,

$$D(k) = \text{Log}_2 \frac{P_{n+s}(k)}{P_n(k)} \quad , \tag{1}$$

where,

$D(k)$ = information content (bits/cycle) at frequency k,

$P_{n+s}(k)$ = relative power at frequency k for the image of interest (including noise), and

$P_n(k)$ = relative power at frequency k for the noise alone.

The resulting information spectrum for the degraded grid image developed earlier is shown in Figure 12. This spectrum is now based on signal-to-noise values and expressed in units of bits of information rather than power. A single measure of content, "information density", can be derived from the spectrum.
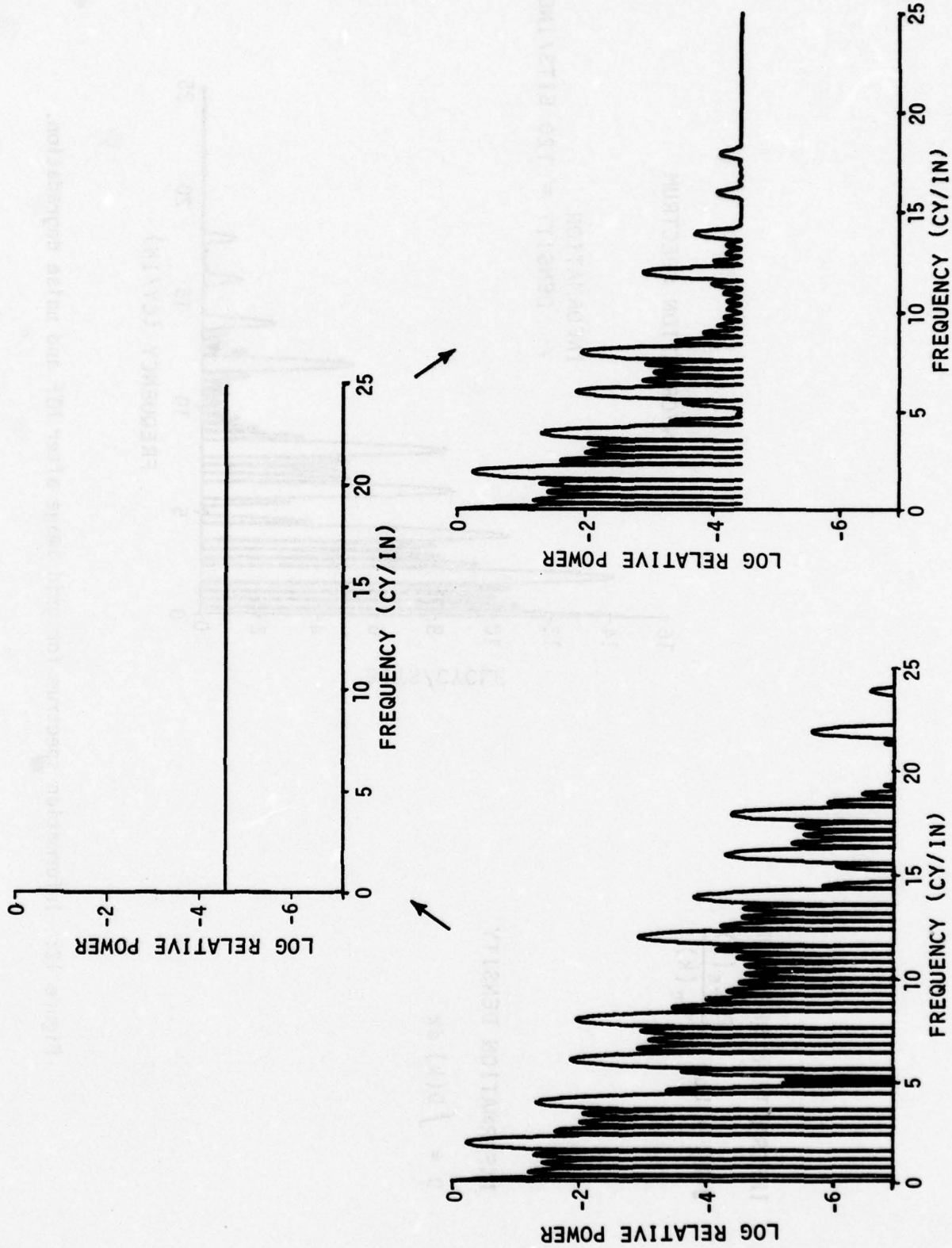
Figure 11: Effect of independent, additive noise on the grid power spectrum.

INFORMATION SPECTRUM

INFORMATION
DENSITY = 120 BITS/INCH

INFORMATION SPECTRUM

$$D(k) = \text{Log}_2 \frac{P_{n+s}(k)}{P_n(k)}$$

INFORMATION DENSITY

$$D = \int D(k) \, dk$$
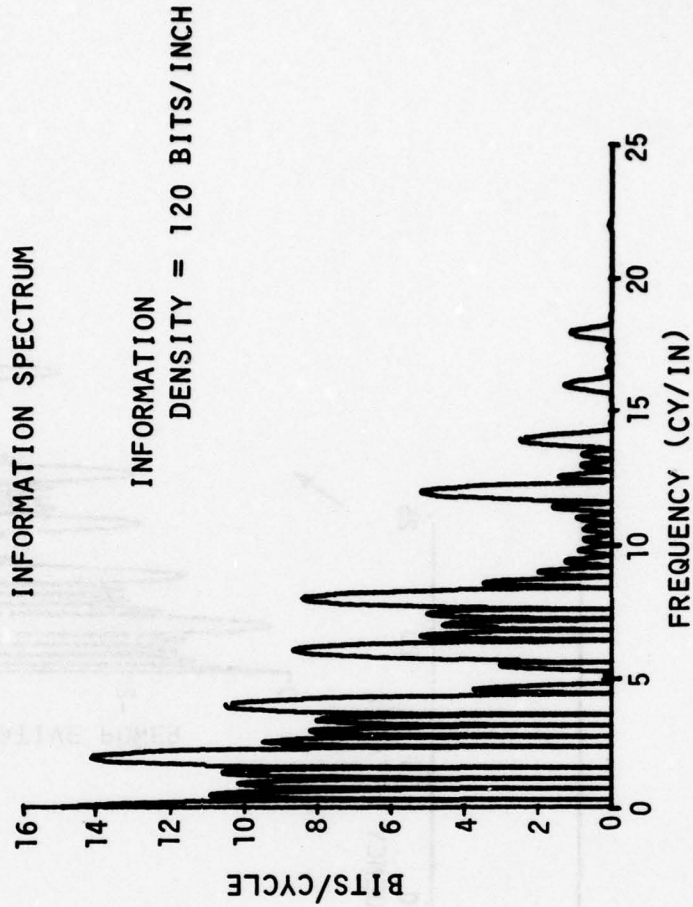
Figure 12: Information spectrum for grid image after MTF and noise degradation.

20

$$D = \int_0^K D(k) \, dk, \qquad\qquad (2)$$

where,

D = information density (bits, per unit length).

The limits of integration are from 0 to K, the maximum useful frequency in the image. The units of length may be in terms of image dimensions (e.g., bits per millimeter) or in terms of target dimensions (e.g., bits per target width.) It is important to note that the formulations expressed by equations (1) and (2) define image information content in the "formal" information theory sense. The resulting values do not reflect the meaning or importance of the interaction of this "information" with the perceptual capabilities of the human observer.

POWER SPECTRUM MEASUREMENT

The examples presented above using a grid pattern are all derived mathematically from the function describing the image content. This is easily done for simple patterns and shapes where describing functions are available. In most practical applications, however, the image of interest is often much too complex to permit description with a single function. In these cases, the image must be digitized or the power spectrum must be measured optically. The latter technique is the primary concern in this study.

The optical power spectrum is a physical measure based on the principles of coherent optical processing. If, as shown in Figure 13, a film transparency is illuminated with coherent, collimated light and the diffracted and non-diffracted light is collected by a lens, then a special pattern of light is produced at the back focal plane of the lens. This is the Fraunhofer diffraction pattern. The distribution of light intensity in this pattern is related to the image Fourier transform and is a function of the orientation, spacing, sharpness and contrast of the edges in the film transparency. It can be shown that,

$$P(k_x, k_y) = \lim_{A = \infty} \langle C \, I \, (k_x, k_y) \rangle \qquad\qquad (3)$$

21
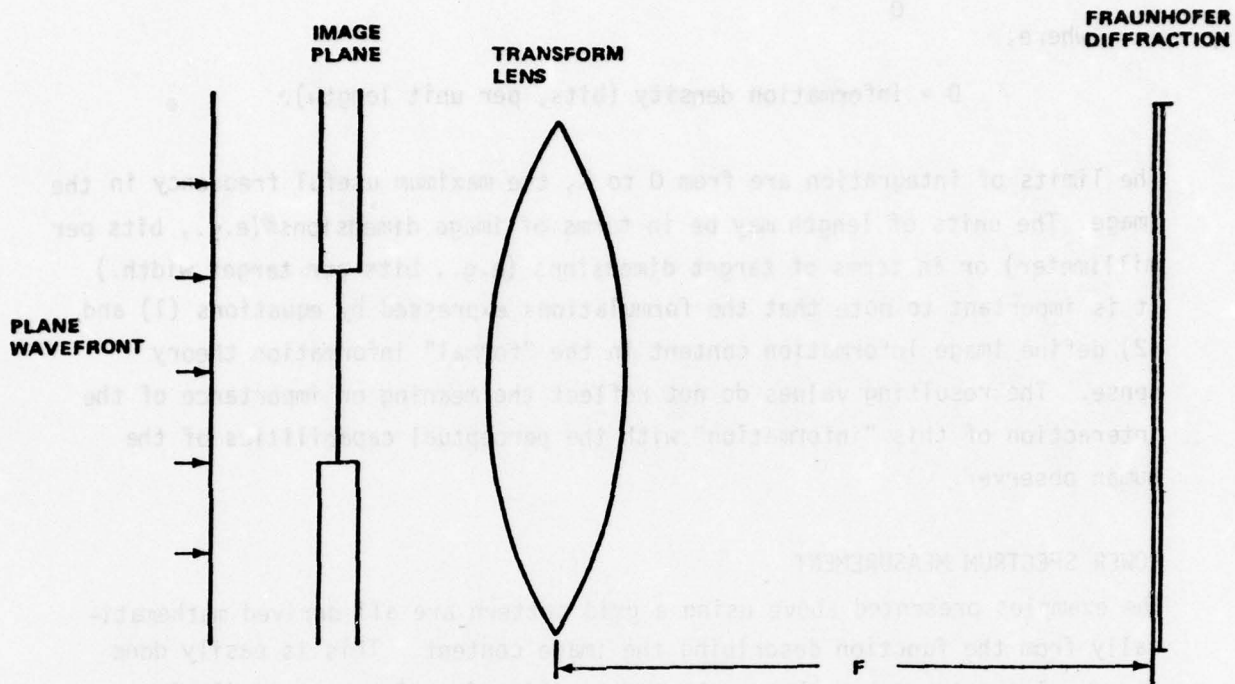
Figure 13: Optical conditions for Fraunhofer diffraction pattern sampling.

where,

$P(k_x, k_y)$ = power per unit area,

k_x, k_y = spatial frequency in x and y axes, respectively, of the image plane

A = image area,

C = a scaling constant, and

$<$ $>$ denotes ensemble average.

$I(k_x, k_y)$ is the intensity of the Fraunhofer diffraction pattern at the point in the pattern related to k_x, k_y by,

$$k_x = u/\lambda F$$
$$k_y = v/\lambda F$$

where,

u, v are coordinates in the diffraction plane,

λ = the wavelength of the illumination source, and

F = the focal length of the "transform" lens.

The theoretical development of the above expressions has been treated extensively in the literature. Goodman (1968), Smith and Thompson (1971) and Ditchburn (1963) provide good sources for this material.

It will be convenient to consider equation (3) in terms of polar coordinates. Thus if we define

$$r = (k_x^2 + k_y^2)^{1/2}, \text{ and}$$
$$\tan^{-1} (k_x/k_y),$$

equation (3) becomes

$$P(r, \theta) = \lim_{A = \infty} \quad < C \, I \, (r, \theta) > \quad . \tag{4}$$

Equation (4) shows that the optical power spectrum is determined by measuring the diffraction pattern intensity distribution. Exact measurement of this distribution is a difficult task because of the large dynamic range

23

(5 to 6 orders of magnitude is a typical range), and for patterns such as shown in Figure 9, very high resolution is required. In order to simplify the measurement and to significantly reduce the resulting data loads, the diffraction pattern distribution is sampled over large areas in the pattern. The detector (Figure 14) is a 64 element array consisting of 32 "rings" and 32 "wedges". Each element is a diffused silicon photodetector on a common substrate. The diffraction pattern is symmetric so the array is split essentially in half, each half measuring a different "characteristic" of the pattern. The rings measure intensity, as a function of radial distance (hence, spatial frequency, r) and the wedges measure intensity as a function of direction, θ. The central ring is a complete circle and measures the zero frequency power. Table 1 lists the dimensions for the individual rings. Table 2 lists the corresponding spatial frequency values with the 40 inch focal length transform lens used in the measurements reported here. For purposes of optical power spectrum measurements, only the ring elements are used. The effect of sampling with the ring elements is to integrate over θ (direction) for discrete spatial frequency bands. As a result, the values obtained represent a gross sampling of the power spectrum, in one dimension, averaged across all possible directions in the image. This approach permits a very rapid measurement rate with minimum data loads. The speed and simplicity, however, are at the expense of losing the fine detail in the true power spectrum.

In addition to the gross sampling effects, there are several error sources inherent in the diffraction pattern sampling process that may reduce the precision and/or validity of the resulting optical power spectrum estimates. The optical power spectrum is a function of the total complex amplitude distribution in the image plane. Image distributions are most commonly expressed in units of intensity transmittance or optical density. Amplitude, as the square root of intensity, will not have the same properties as the more common units. This is particularly relevant to assumptions about linearity and additivity in the subsequent applications of the power spectrum data. Because of the dependence on complex amplitude, the power spectrum is sensitive to phase effects introduced by irregularities in the film thickness. In the measurement process, an aperture is used to limit the image area being measured. The power spectrum of the aperture is convolved with the image contribution in the total power spectrum. In addition, as with any optical system, scatter of light by

24
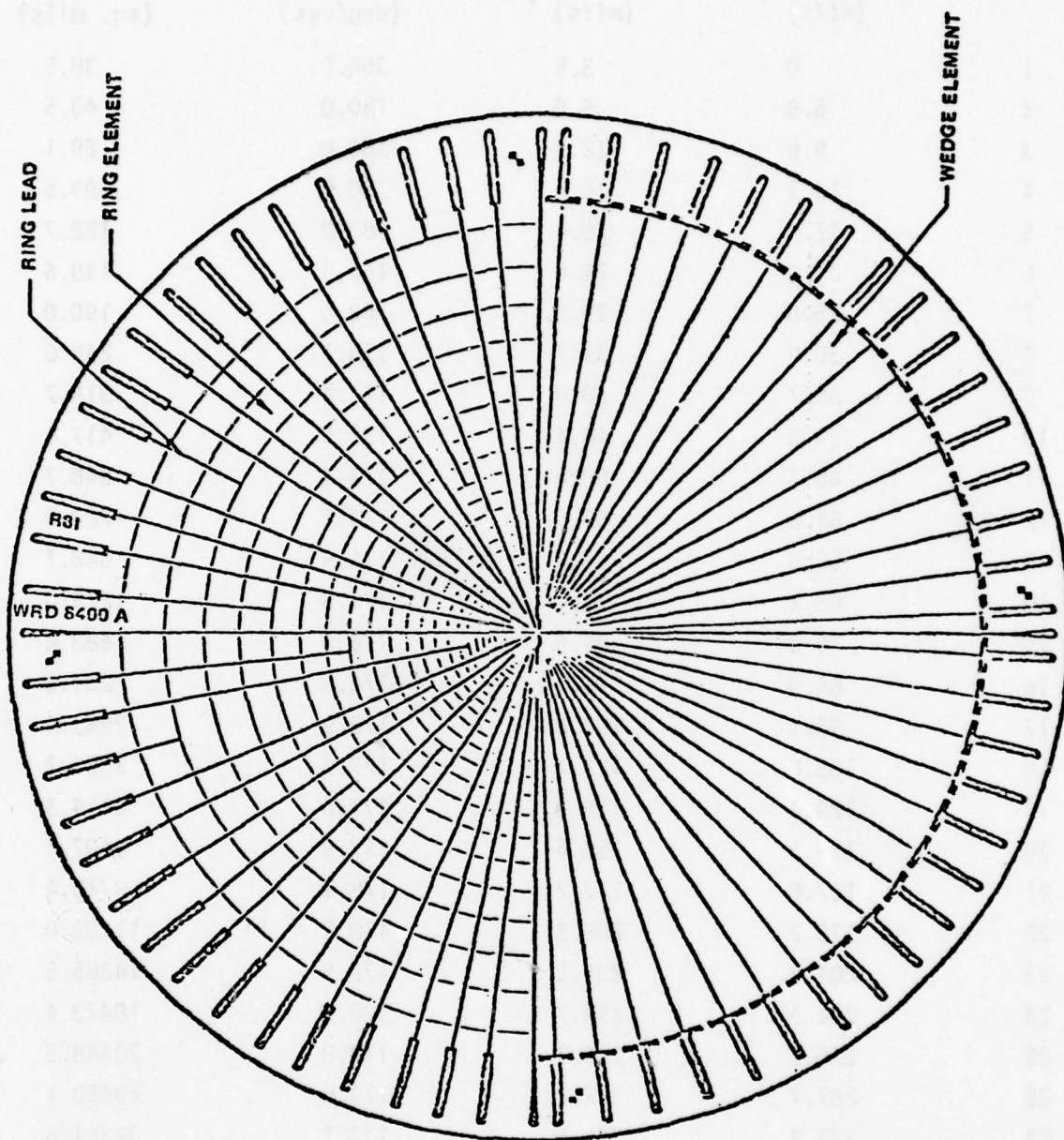
Figure 14: Segmented photodetector used for diffraction pattern sampling.

Table 1: Detector Ring Dimensions

Ring No.	Minimum Radius (M_i) (mils)	Maximum Radius (N_i) (mils)	Ring Angle (Ψ_i) (degrees)	Total Effective Area (A_i) (sq. mils)
1	0	3.5	360.0	38.5
2	5.8	8.6	180.0	43.5
3	9.6	12.5	180.0	69.1
4	13.5	16.4	180.0	93.5
5	17.4	20.4	180.0	122.7
6	21.4	24.6	166.3	148.6
7	25.6	29.0	168.5	190.0
8	30.0	33.7	170.1	245.0
9	34.7	38.8	171.4	318.7
10	39.8	44.4	172.5	417.4
11	45.4	50.6	173.4	548.7
12	51.6	57.5	174.2	722.0
13	58.5	65.2	174.9	948.7
14	66.2	74.0	175.5	1279.6
15	75.0	83.9	176.0	1688.8
16	84.9	95.1	176.5	2237.0
17	96.1	107.8	176.9	2963.6
18	108.8	122.1	177.3	3884.7
19	123.1	138.3	177.6	5114.3
20	139.3	156.6	177.9	6697.1
21	157.6	177.2	178.1	8715.4
22	178.2	200.2	178.3	11209.0
23	201.2	225.9	178.5	14385.5
24	226.9	254.7	178.7	18473.4
25	255.7	286.7	178.8	23448.5
26	287.7	322.2	179.0	29630.1
27	323.2	361.6	179.1	37361.6
28	362.6	405.0	179.2	46614.1
29	406.0	452.8	179.3	57988.0
30	453.8	505.4	179.3	71889.4
31	506.4	563.0	179.4	88448.7
32	564.0	626.0	179.5	108409.8

26

Table 2: Detector Spatial Frequency Values

40 inch Focal Length

Ring No.	Minimum Frequency (cy/mm)	Maximum Frequency (cy/mm)	Center Frequency (cy/mm)	Bandwidth (cy/mm)
1	0.00	0.14	0.07	.14
2	0.23	0.34	0.28	.11
3	0.38	0.49	0.43	.11
4	0.53	0.65	0.59	.12
5	0.69	0.80	0.75	.11
6	0.85	0.97	0.91	.12
7	1.01	1.15	1.08	.14
8	1.18	1.33	1.26	.15
9	1.37	1.51	1.44	.14
10	1.57	1.75	1.66	.18
11	1.79	2.00	1.89	.21
12	2.03	2.27	2.15	.24
13	2.31	2.57	2.44	.26
14	2.61	2.92	2.76	.31
15	2.96	3.31	3.13	.35
16	3.35	3.75	3.55	.40
17	3.79	4.25	4.02	.46
18	4.29	4.81	4.55	.52
19	4.85	5.45	5.15	.60
20	5.49	6.17	5.83	.68
21	6.22	6.99	6.60	.77
22	7.03	7.90	7.46	.87
23	7.93	8.91	8.42	.98
24	8.95	10.05	9.49	1.10
25	10.08	11.31	10.69	1.23
26	11.34	12.70	12.02	1.36
27	12.75	14.26	13.50	1.51
28	14.30	15.97	15.13	1.67
29	16.01	17.85	16.93	1.84
30	17.89	19.93	18.91	1.96
31	19.97	22.20	21.08	2.23
32	22.24	24.68	23.46	2.44

27

the various optical components adds noise to the measured values. Evaluations of these error sources are reported in the previous study by Schindler and Martin (1978).

PREVIOUS RESULTS

The successful use of coarse sampling of the Fraunhofer diffraction pattern for a number of applications has been reported in the literature. The range of applications includes automatic pattern recognition, image quality determination and cloud cover analysis. Studies by Lendaris and Stanley (1970), Jensen (1973), Nill (1976), Leachtenauer (1977), Kasdan (1977) and Lukes (1977) all used a small number of sampling intervals (between 8 and 64) to characterize the diffraction pattern light distribution.

The previous effort, Schindler and Martin (1978), was concerned with the evaluation of this technique in a series of studies using CRT displays. In these studies, several display operating parameter values were varied including dynamic range, bandwidth, noise level and quantization level in digitized imagery. The effects of these variations on the measured power spectra expressed as information density and on observer target recognition performance were determined. The relationship between information density and observer performance was then evaluated.

Target recognition performance was measured using a series of "zoom" sequences of tactical military vehicles. The visual angle of the vehicle at recognition was used as the measure of performance. Information density measures were made using standardized inputs (random dot and random bar patterns) as well as the vehicle images used in the performance test. Since the measurement technique requires the use of photographic transparencies, the CRT images were recorded on film for the information density measurements.

The results generally supported the effectiveness of the information density measures. The values for the random dot and random bar patterns show very strong positive relationships with CRT dynamic range and bandwidth. Product-moment correlation coefficients for the dot pattern, for example, were 0.997

with log dynamic range and 0.98 with log bandwidth. The random bar results were comparable. Information density values for the vehicle images correlated less strongly, 0.90 and 0.88 with log dynamic range and log bandwidth respectively. Differences due to noise levels and number of quantization levels used in the studies were too small to establish significant relationships.

The relationships between information density and observer target recognition performance are more variable than those with display parameters but are sufficiently strong to demonstrate a high degree of promise for the diffraction pattern sampling approach. Product-moment correlation coefficients across all three performance studies exceeded 0.90. These results are summarized in Figure 15. The information density values in this plot have been transformed to bits per square degree to reflect the solid viewing angle referenced to the observer. Conventional analog TV imagery was used for Studies I and II while digitized TV imagery was used for Study III.
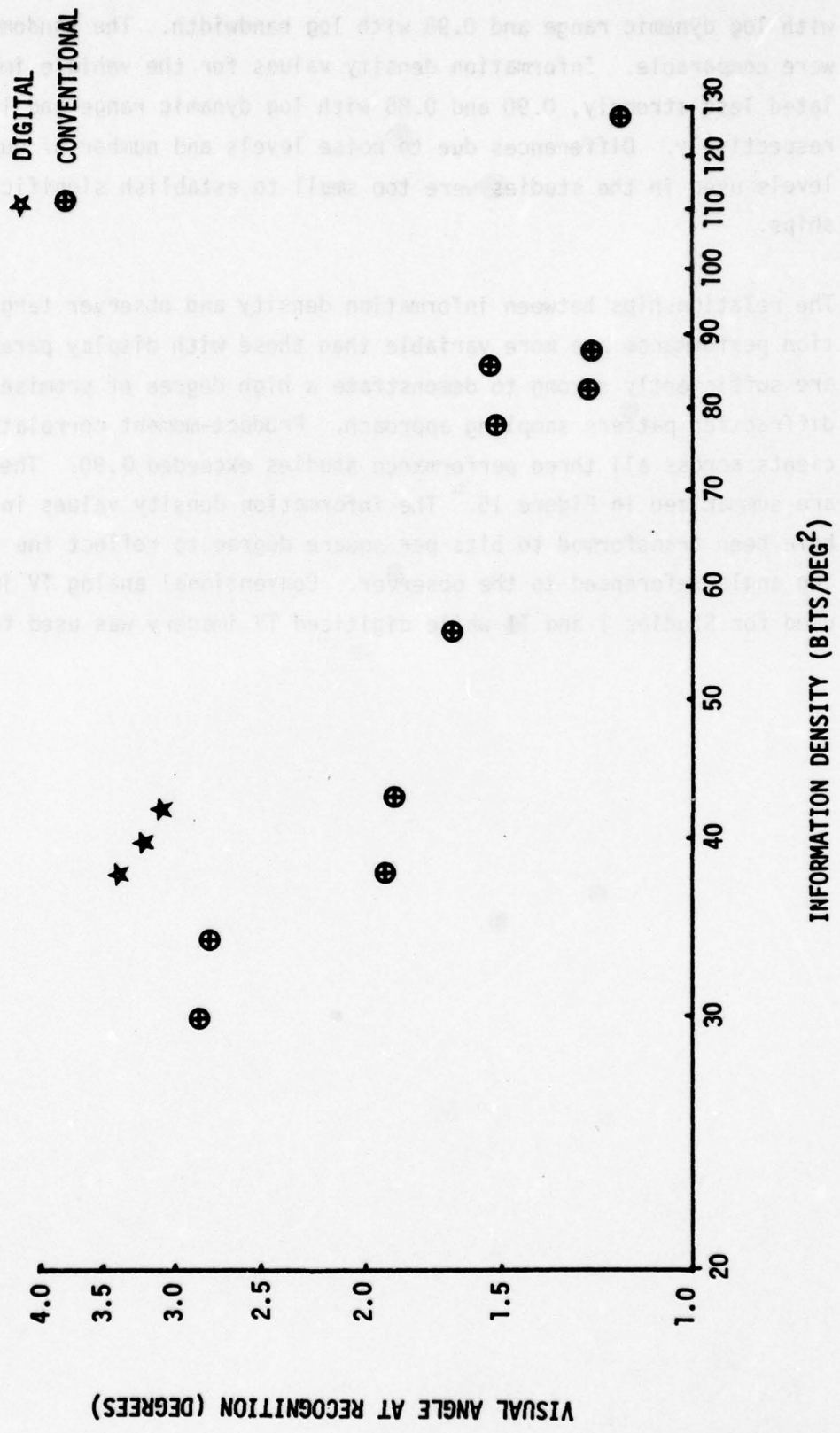
SECTION III

OBJECTIVES AND APPROACH

The ultimate goal addressed by this study is the development of a systematic, quantitative approach for the application of digital image processing. The specific objective is to examine the use of optical power spectrum sampling and information theory metrics as potential tools for such an application. Two questions are addressed by the study:

1) Does the OPS/information density measure "properly" reflect the impact of digital image processing?

2) Can the OPS/information density measure contribute to the selection and implementation of digital processing techniques?

The approach selected for determining answers to these questions involves the following steps:

1) Select an image sample that is relevant to problems of practical interest and representative of conditions encountered in the real world.

2) Select digital image processing techniques that are representative of state-of-the-art applications of this technology.

3) Apply the selected processing techniques to the baseline imagery.

4) Measure the OPS/information density values for the imagery processed under each condition and compare with measures for the unprocessed imagery.

5) Measure operator target recognition performance for processed and unprocessed imagery.

6) Relate OPS/information density values to changes in recognition performance due to processing.

7) Determine decision criteria for selecting processing techniques.

The baseline imagery selected for this study utilized a terrain table with models of tactical military vehicles. Five vehicles were used as shown in Figure 16, each at three average reflectance values (53%, 33%, and 26%). The average reflectance of the background was measured at 40%. Each of the 15 conditions (5 targets x 3 reflectance levels) were recorded at five simulated scales (1:4675, 1:4110, 1:2928 and 1:2363). Detailed descriptions of the imagery and its preparation are presented in the following section.

Five processing conditions are used in this study:

1) No processing

2) Histogram equalization

3) "J.N.D." equalization

4) Linear frequency filtering

5) "Homomorphic" frequency filtering

These techniques are described in the previous section.

Target recognition performance is measured with a "forced choice" procedure, i.e., the observer is required to respond with one of the target names. Percent correct responses is used as the measure of observer recognition performance.

In addition to observer performance measures, the information density of each image is determined with optical power spectrum sampling. The basic design is therefore a covariate approach with performance and information density as dependent variables and target reflectance, image scale and processing as independent variables.

32

Figure 16: Examples of the five vehicle images.

SECTION IV

IMAGE ACQUISITION AND PROCESSING

Figure 17 depicts the image acquisition conditions for the five scale levels used in this study. The terrain and vehicle models are at a scale of 1:87. The images acquired by the television camera (General Electric Model ED 6073B, 525 line with a 12 mm focal length Elgert f2.0 lens) were recorded on a video disc. The primary light source was a photo-flood lamp positioned 56 inches above the terrain board with supplemental lighting from overhead flourescent lamps. For the target imagery, 75 frames (5 targets x 5 scales x 3 reflectance levels) were recorded. Reflectance level was varied by painting the models with grey, olive drab and black paint. In addition, the models were dusted with fine, dry earth to reduce specular reflections. Along with the target images, 5 standardized targets were recorded. These consisted of a random width bar target at vertical, horizontal and diagonal orientations; a random dot target; and a uniform grey target at the average scene reflectance value. The latter target provides the input for image noise measurements in the information density calculations.

Each of the images were digitized from the video disc. Digitization was at 256 grey levels (8 bits) and each image was formatted as a 32 x 32 element array. The digitized data were recorded on magnetic tape for processing. Four processing algorithms were used as described in Section II.

        1) Histogram Equalization

        2) "J.N.D." Equalization

        3) Linear Frequency Filtering

        4) Hormomorphic Frequency Filtering

All of the data processing was performed with an Interdata Computer, Model 8/32. The processed data was recorded on magnetic tape for hardcopy printing with a laser beam recorder.

Figure 17: Image recording geometry.
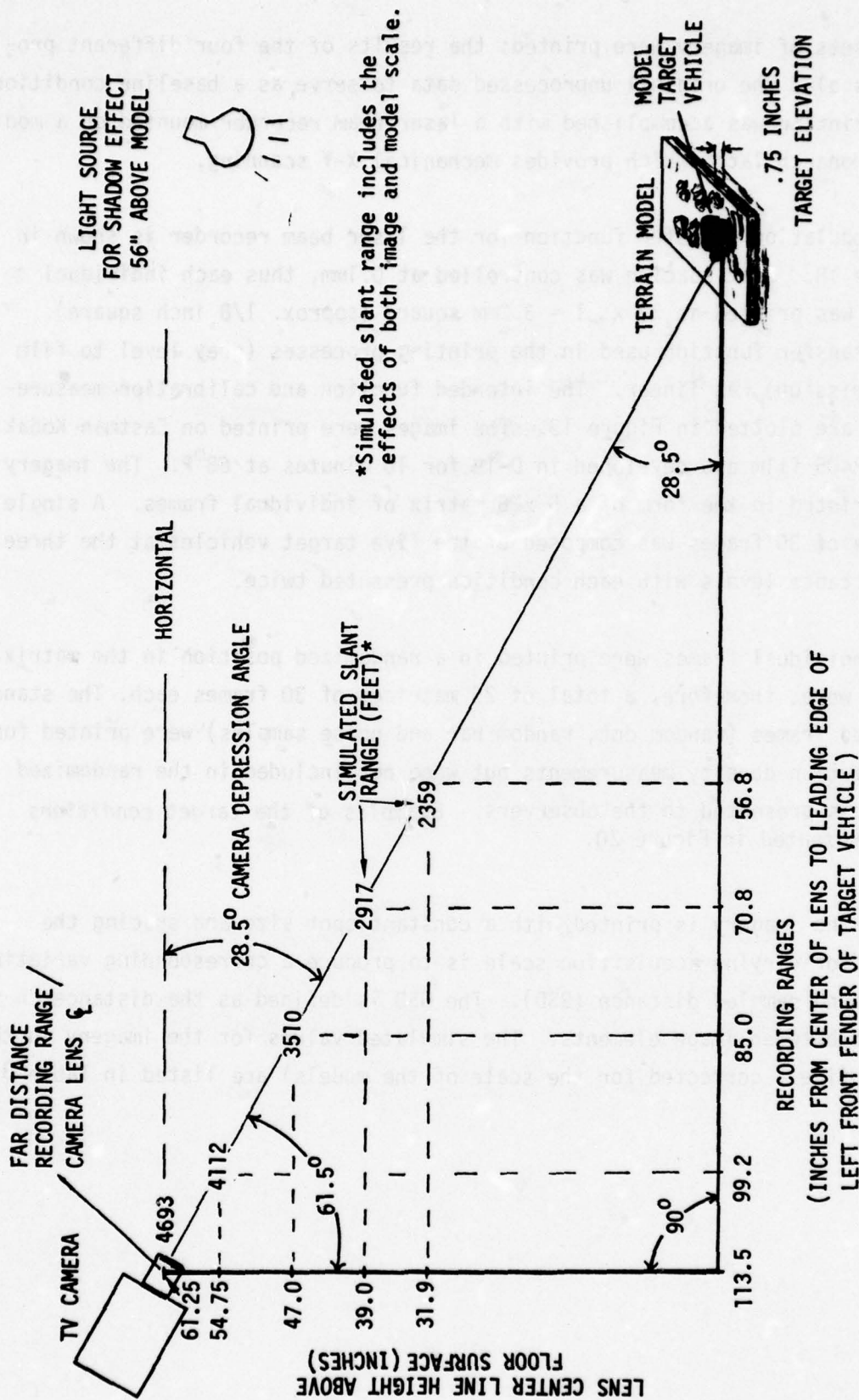
*Simulated slant range includes the effects of both image and model scale.

LIGHT SOURCE
FOR SHADOW EFFECT
56" ABOVE MODEL

MODEL
TARGET
VEHICLE

TERRAIN MODEL

.75 INCHES
TARGET ELEVATION

28.5°

HORIZONTAL

28.5° CAMERA DEPRESSION ANGLE

SIMULATED SLANT
RANGE (FEET)*

2359
2917
3510
4112
4693

56.8
70.8
85.0
99.2
113.5

RECORDING RANGES
(INCHES FROM CENTER OF LENS TO LEADING EDGE OF
LEFT FRONT FENDER OF TARGET VEHICLE)

90°

61.5°

FAR DISTANCE
RECORDING RANGE
CAMERA LENS ℄

TV CAMERA

61.25
54.75
47.0
39.0
31.9

LENS CENTER LINE HEIGHT ABOVE
FLOOR SURFACE (INCHES)

Five sets of imagery were printed; the results of the four different processes plus the original unprocessed data to serve as a baseline condition. The printing was accomplished with a laser beam recorder mounted on a modified Monarch lathe which provides mechanical X-Y scanning.

The modulation transfer function for the laser beam recorder is shown in Figure 18. Spot spacing was controlled at 0.1mm, thus each individual image was printed as 32 x .1 = 3.2mm square (approx. 1/8 inch square). The transfer function used in the printing processes (grey level to film transmission) was linear. The intended function and calibration measurements are plotted in Figure 19. The images were printed on Eastman Kodak type 2405 film and developed in D-19 for 10 minutes at 68°F. The imagery was printed in the form of a 5 x 6 matrix of individual frames. A single matrix of 30 frames was composed of the five target vehicles at the three reflectance levels with each condition presented twice.

The individual frames were printed in a randomized position in the matrix. There were, therefore, a total of 25 matrices of 30 frames each. The standardized frames (random dot, random bar and noise samples) were printed for information density measurements but were not included in the randomized matrices presented to the observers. Examples of the target conditions are presented in Figure 20.

Since the imagery is printed with a constant spot size and spacing the effect of varying acquisition scale is to produce a corresponding variation in ground sampled distance (GSD). The GSD is defined as the distance on the ground between image elements. The simulated values for the imagery in this study (i.e., corrected for the scale of the models) are listed in Table 3.
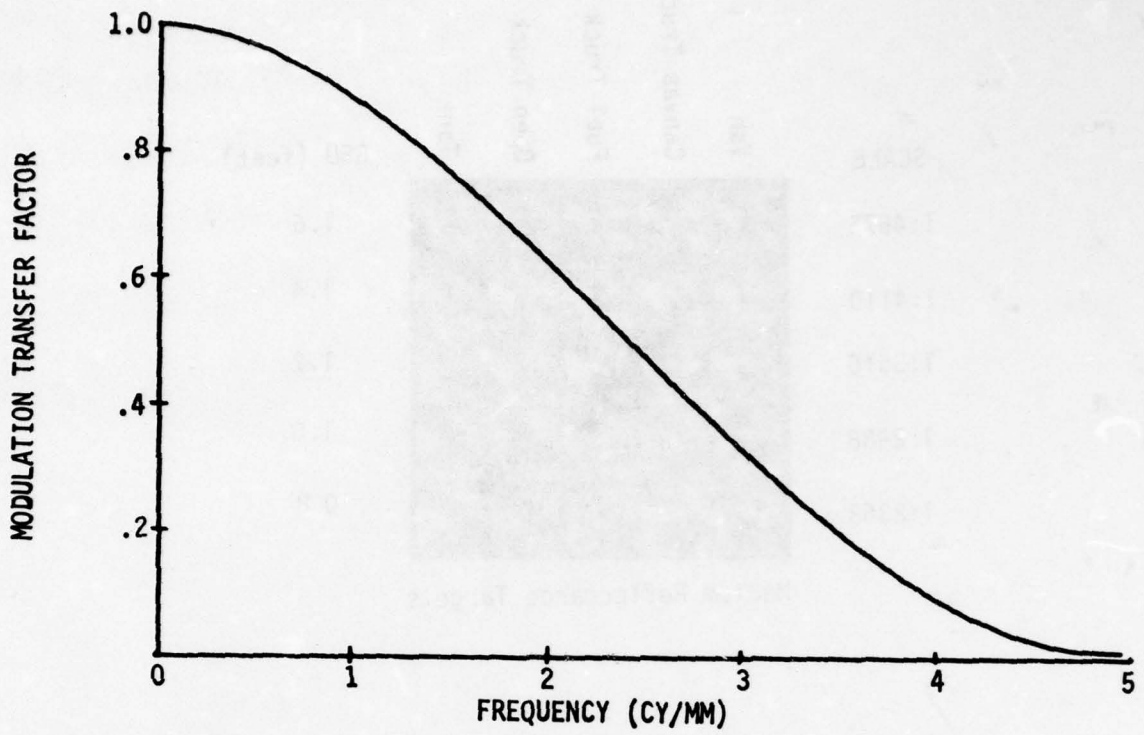
Figure 18: Laser beam recorder modulation transfer function.
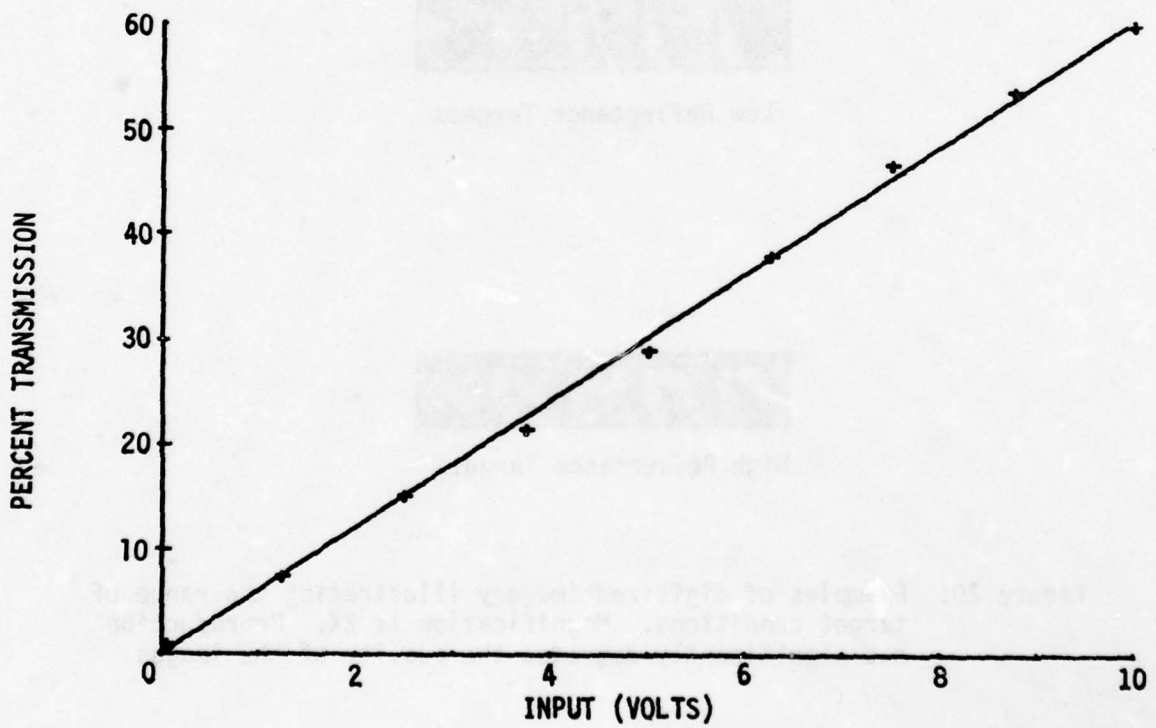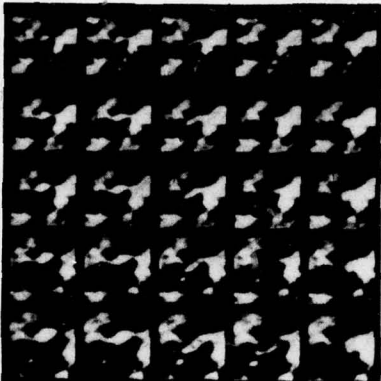
Figure 19: Image printing transfer function.

37

SCALE | Van | Canvas Truck | Fuel Truck | Open Truck | Tank | GSD (feet)

1:4675 — 1.6

1:4110 — 1.4

1:3510 — 1.2

1:2988 — 1.0

1:2363 — 0.8

Medium Reflectance Targets

Low Reflectance Targets

High Reflectance Targets

Figure 20: Examples of digitized imagery illustrating the range of target conditions. Magnification is 2X. Reproduction has significantly degraded the quality of the images.

TABLE 3: SIMULATED SCALE AND GROUND SAMPLED DISTANCES

IMAGE SCALE	GROUND SAMPLED DISTANCE (feet)
1:4675	1.6
1:4110	1.4
1:3510	1.2
1:2988	1.0
1:2363	0.8

The corresponding visual angles for the 12-inch viewing distance used in the performance tests are also indicated. Table 4 lists the average target reflectance values for the three levels used.

Corresponding image contrast values are included based on a measured average background reflectance of 0.40. Contrast is calculated as,

$$C = \frac{R_T - R_B}{R_B}$$

where R_T = average target reflectance
R_B = average background reflectance

TABLE 4: TARGET REFLECTANCE AND IMAGE CONTRAST VALUES

LEVEL	TARGET REFLECTANCE	CONTRAST*
Low	26%	-.35
Medium	33%	-.18
High	53%	.32

(*based on average background reflectance of 40%)

Image sizes for the individual targets as printed are listed in Table 5.

TABLE 5: VEHICLE IMAGE DIMENSIONS

(*Calculated for 12-inch viewing distance)

G.S.D. (FT)	TARGET	LENGTH (mm)	WIDTH (mm)	VISUAL ANGLE* (MIN) LENGTH	WIDTH	ELEMENTS PER TARGET WIDTH
1.6	CANVAS	1.61	.82	18.2	9.2	8.2
	OPEN	1.57	.71	17.7	8.0	7.1
	VAN	1.60	.86	18.0	9.7	8.6
	FUEL	1.52	.63	17.1	7.1	6.3
	TANK	1.19	.73	13.4	8.2	7.3
1.4	CANVAS	1.83	.93	20.6	10.5	9.3
	OPEN	1.78	.80	20.1	9.0	8.0
	VAN	1.82	.98	20.5	11.1	9.8
	FUEL	1.72	.72	19.4	8.1	7.2
	TANK	1.35	.83	15.2	9.4	8.3
1.2	CANVAS	2.14	1.09	24.1	12.3	10.9
	OPEN	2.09	.94	23.6	10.6	9.4
	VAN	2.13	1.14	24.0	12.9	11.4
	FUEL	2.02	.84	22.8	9.5	8.4
	TANK	1.58	.98	17.8	11.1	9.8
1.0	CANVAS	2.57	1.31	29.0	14.8	13.1
	OPEN	2.50	1.13	28.2	12.7	11.3
	VAN	2.56	1.37	28.9	15.5	13.7
	FUEL	2.42	1.01	27.3	11.4	10.1
	TANK	1.90	1.17	21.4	13.2	11.7
0.8	CANVAS	3.18	1.62	35.9	18.3	16.2
	OPEN	3.10	1.40	35.0	15.8	14.0
	VAN	3.17	1.70	35.8	19.2	17.0
	FUEL	3.00	1.25	33.8	14.1	12.5
	TANK	2.35	1.45	26.5	16.4	14.5

SECTION V

OBSERVER PERFORMANCE TESTING

OBJECTIVE

Observer target recognition performance was measured with the baseline
and processed imagery to provide criterion values for evaluating the
effectiveness of the processing techniques used in this study. The re-
sulting performance measures are also important for evaluating the rela-
tionship between the information density measures and observer perform-
ance.

OBSERVERS

Fifteen subjects, all Boeing employees, (12 male, 3 female) were used
in the performance testing. All observers were experienced in visual per-
formance testing, although not necessarily in target image recognition.
Ages ranged from 25 to 48. Near point visual acuity (14 inches), tested with
an American Optical Sight-Screener, was 20/20 or better for all observers.

PERFORMANCE TASK

The imagery, described in Section IV, consists of 25 matrices. Each
matrix contains 30 individual vehicle images (5 types, 3 reflectance
levels, 2 replications). The image set consists of one matrix for each
processing by scale condition. A forced-choice identification procedure
was used. The observer was required to respond with the identification of
the target type even if it was a best guess. The proportion of correct
responses out of the 30 images in each matrix was taken as the measure of
performance.

VIEWING CONDITIONS

Each image (5 x 6 matrix) was viewed on a light box. The light box pro-
vides a diffuse light source with a measured luminance of 320 foot-Lamberts.
Since the average transmission of the imagery is approximately 30%, the

average scene luminance as presented to the observer was about 100 foot-Lamberts. In order to provide the desired range of target visual angles, a 12 inch viewing distance was used. A head and chin rest was mounted in front of the light box to assure that a constant 12 inch viewing distance was maintained by all observers throughout the test sequence. Ambient luminance in the test room was maintained at 5 foot-Lamberts. At a 12 inch viewing distance, the visual angles of the individual targets are as shown in Table 5 (page 40). The overall matrix, including borders, subtends 3.3 degrees horizontally and 3.9 degrees vertically.

TEST PROCEDURE

After the initial acuity check with the Sight Screener, each observer was briefed on the general objectives of the performance test and provided with a description of the imagery to be presented. A set of detailed photographs of the target vehicles was presented and the proper identification described. These photographs were available to the observer throughout the testing session. After demonstrating familiarity with the individual target identities, the observer was presented with a series of training images. These images provided examples of the range of image conditions with respect to vehicle type reflectance and image scale. Observers were requested to identify the vehicles, with feedback, for a total of 120 trials. After training, a pretest was administered using a baseline imagery at the largest scale. A criterion proportion of 0.80 was required before actual testing began.

The order of presentation during the actual test was fixed with respect to scale. All observers were presented with the smallest scale first and the sequence proceeded through increasing scales. This was done to guard against the possibility of learning extraneous cues, if they existed, from the easier imagery. Within each scale condition, the imagery was presented in a balanced order with respect to processing condition. No time limit was imposed on the observer's response. Observers were free to use the target reference photographs at any time during the testing session.

RESULTS

Average performance scores as a function of processing condition and scale are presented in Table 6. The values in parentheses are "corrected for

42

Table 6: Observer Target Recognition Performance

Scale	Baseline	Histogram Equalization	Processing Condition J.N.D. Normalization	Linear Freq. Filtering	Logarithms Freq. Filtering
1:4675	.34 (.18)*	.42 (.28)	.36 (.20)	.35 (.18)	.35 (.19)
1:4110	.45 (.32)	.44 (.30)	.41 (.26)	.40 (.25)	.38 (.23)
1:3510	.46 (.32)	.49 (.36)	.52 (.40)	.41 (.26)	.47 (.34)
1:2928	.60 (.50)	.58 (.48)	.66 (.57)	.56 (.46)	.59 (.49)
1:2363	.79 (.74)	.76 (.70)	.78 (.73)	.66 (.57)	.71 (.63)

*Values in parentheses are corrected for guessing (see text)

guessing". This correction uses the transformation recommended by
Guilford (1954) and is intended to compensate for the fact that the sub-
ject knows that only five target types are being presented. He could,
therefore, achieve a performance level of 0.20 without even looking at
the imagery. The transformation used is,

$$P_C = \frac{A}{A-1} \left(P_0 - \frac{1}{A} \right),$$

where,

P_C = proportion corrected for guessing,
A = the number of alternative responses (five in
this study), and
P_0 = the observed proportion.

Results of the analysis of variance for the corrected data are summarized
in Table 7.

Table 7: Performance Score Analysis of Variance Summary

Source	Degrees of Freedom	Sum of Squares	Mean Square	Error Term	F
Observers	14	17.95	1.27	OxSxP	42.33*
Scale	4	28.84	7.21	OxS	721.00*
Process	4	1.08	0.27	OxP	9.00*
OxS	56	5.52	0.10	OxSxP	3.33*
OxP	56	1.66	0.03	OxSxP	1.00
SxP	16	1.84	0.12	OxSxP	4.00*
OxSxP	224	5.95	0.03		
Total	374	64.64	0.17		

*Significant result ($\rho \leq .05$).

In keeping with standard statistical practice for analysis of proportions, the
transformation,

$$y = \text{arcsine } \sqrt{X},$$

44

was used. In the analytic model used, observers are considered to be
a random sample of the population of possible observers. This constraint
requires the use of the error terms as shown in the table.

The results show all main effects to be significant at the 0.05 level
as well as the observer-by-scale and scale-by-processing condition inter-
actions. Significant differences among observers is a common finding in
visual performance studies. No obvious relationships between performance
level and observer age, sex or experience were observed.

The overall effect of scale is plotted in Figure 21. It is clear from the
figure that, as expected, the effect of scale is substantial and appears
linear. It is important to recall, however, that ground sampled
distance is confounded with scale and the effects of these parameters can-
not be separated in this study. The performance values can also be related
to the number of picture elements per target width as follows.

$$\text{No. of elements/tgt. width} = 11.95/GSD.$$

This transformation is based on the average target width.

The overall means for the processing conditions are shown in Table 8.

Table 8: Overall Processing Effects on Performance

Processing Condition	Performance* (average proportion of correct responses)
Baseline	.41
Histogram Equalization	.42
J.N.D. Normalization	.43
Linear Frequency Filtering	.34
Logarithmic Frequency Filtering	.38

*corrected for guessing

The Duncan Multiple Range Test for these means shows that performance levels
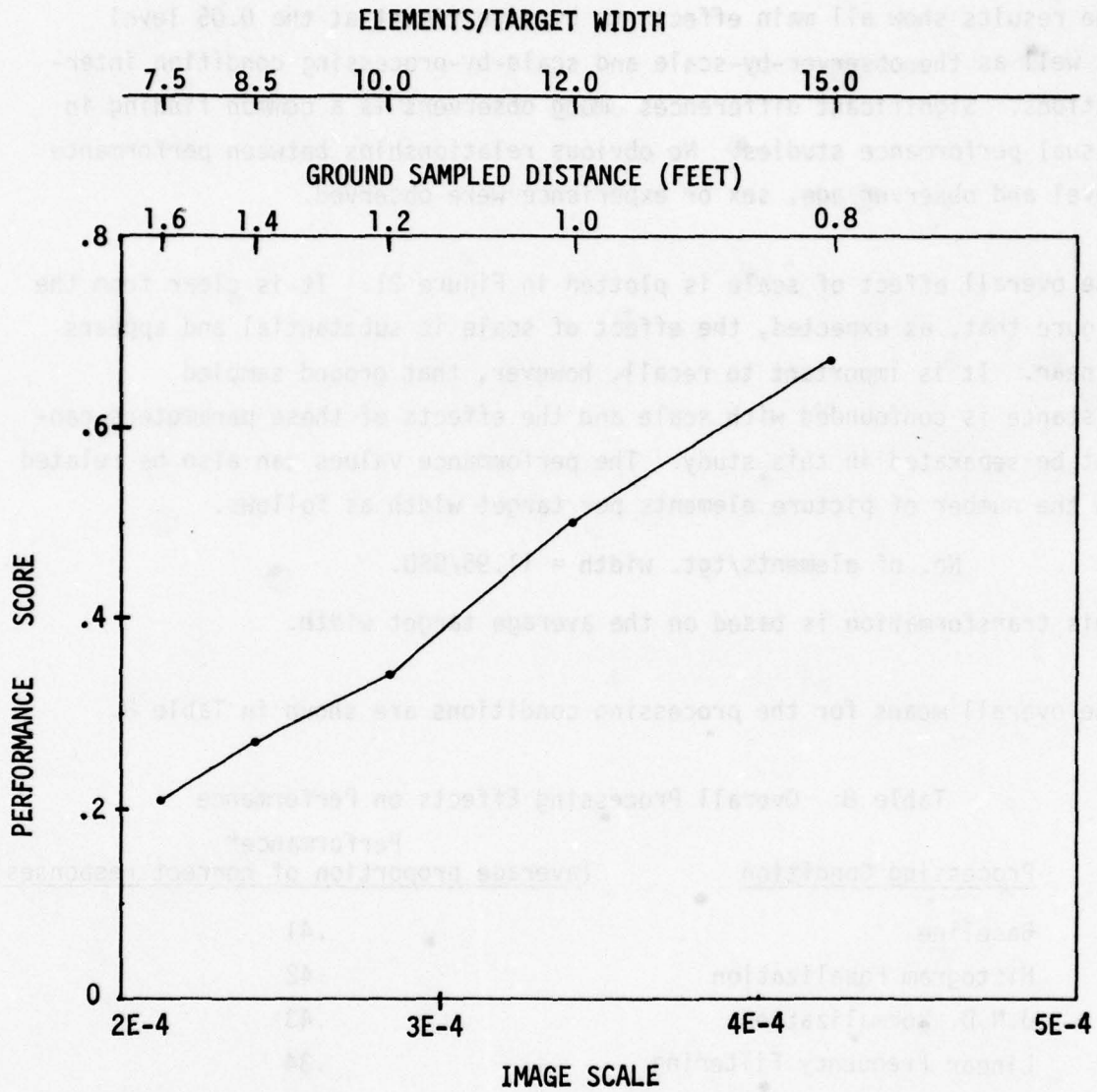for the baseline, histogram equalization and J.N.D. normalization do not differ

45

Figure 21: Scale effects on observer performance.

significantly. Both of the spatial filtering conditions are significantly
different from all others. Interpretation of these results, however, must
consider the significant interaction with scale. This situation is depicted
in Figure 22 for the histogram modification techniques and in Figure 23 for
the filtering techniques. Although their overall means do not differ signi-
ficantly from the baseline, the two histogram modification techniques show
significant improvements at the middle scale (1:3510). J.N.D. normalization
also shows improvement at the next larger scale (1:2928). Compared with the
baseline, the linear spatial filter shows a decline in performance at all
but the smallest scale (1:4675). It must be noted that these results are
not to be interpreted as a definitive test of the specific processing tech-
niques used here. The processing and test conditions used are too restrict-
ive to permit broad generalization of the processing effectiveness results.

In a separate analysis, the performance tests were rescored to permit an
evaluation of the effects of target reflectance. The results are presented
in Figure 24 as performance changes from the baseline condition. The results
show very little change for the low reflectance targets. The medium reflect-
ance (minimum contrast) targets produce large improvements with all but the
linear spatial filter. The high reflectance targets show significant degrada-
tions in performance with the possible exception of J.N.D. normalization.
The latter result suggests that the contrast stretching employed in all four
processing techniques overcompensated at the bright end of the range and
saturated the brighter target details. Visual examination of the test imag-
ery supports this suggestion.

These results have important implications for the evaluation and application
of digital image processing techniques. Optimizing a technique for a speci-
fic target reflectance or contrast may not provide effective performance at
other levels. Since target contrast will vary with a number of factors, an
effective processing technique should be broad in its range of application.
Certainly it should not degrade performance as seen in the results here. A
proper evaluation, therefore, should include a representative range of target
contrasts. Such was the motivation for the range of reflectance levels used
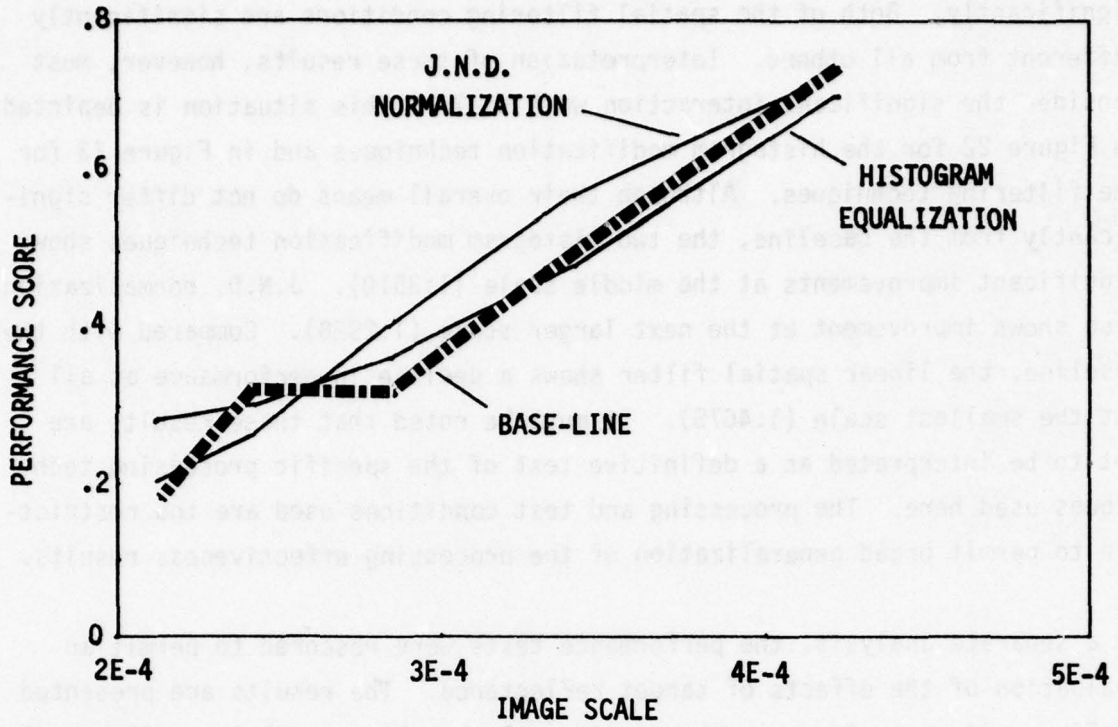in this study.

47

Figure 22: Histogram modification effects as influenced by scale.
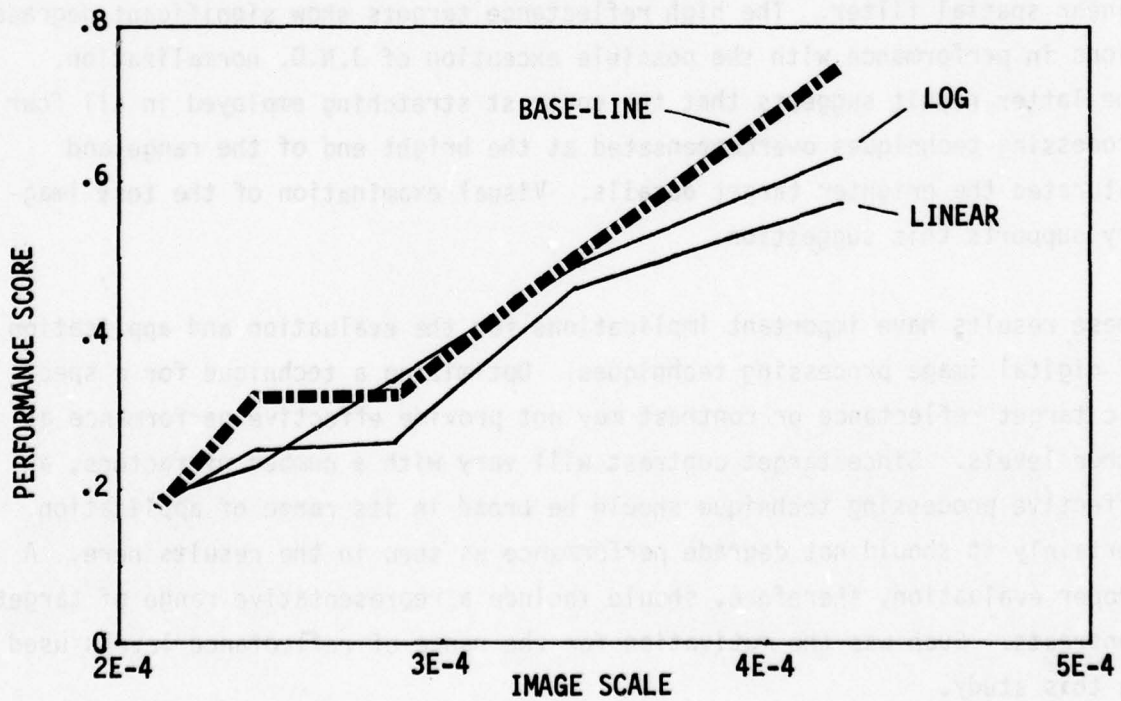

Figure 23: Frequency filtering effects as influenced by scale.

48

LOW REFLECTANCE TARGETS

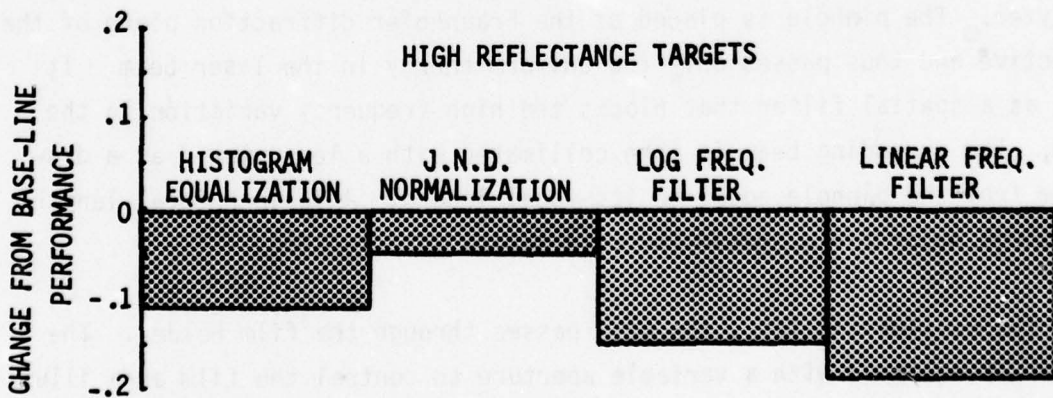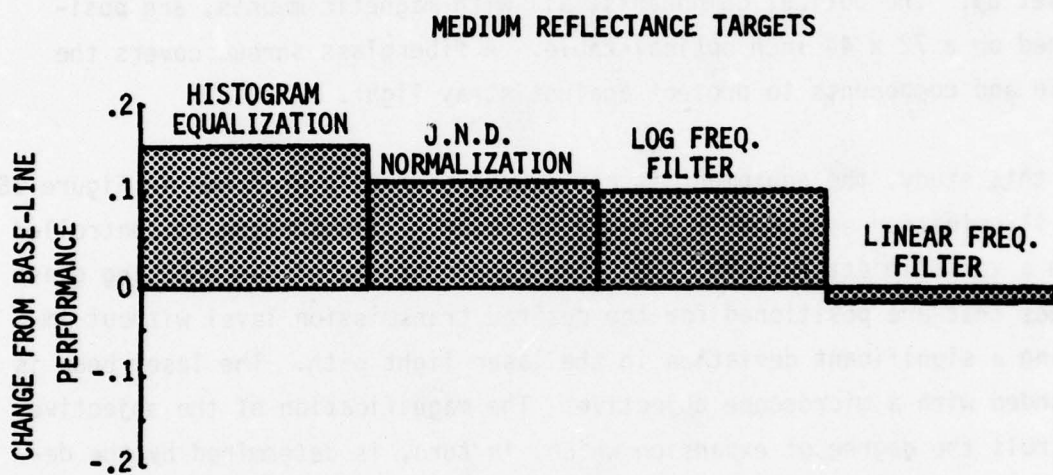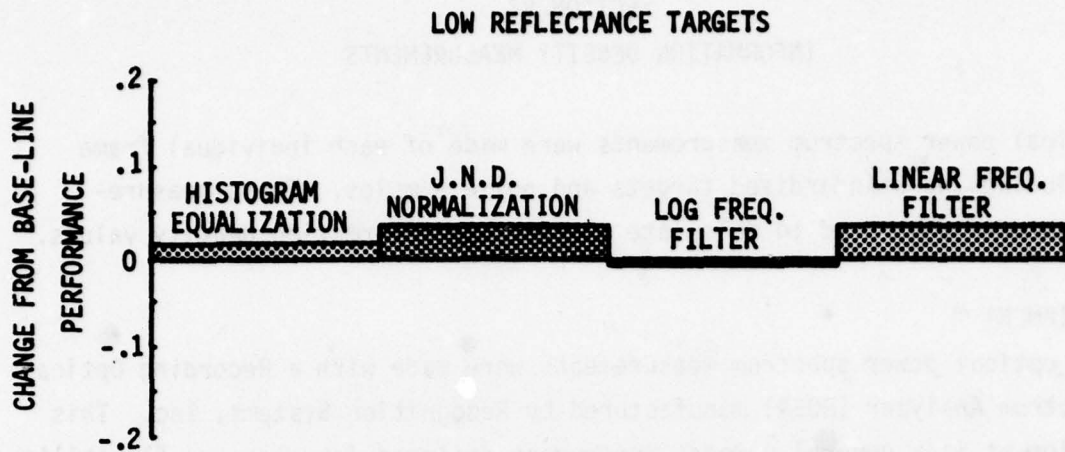
MEDIUM REFLECTANCE TARGETS

HIGH REFLECTANCE TARGETS

Figure 24: Influence of target reflectance on processing effectiveness.

SECTION VI
INFORMATION DENSITY MEASUREMENTS

Optical power spectrum measurements were made of each individual frame
including the standardized targets and noise samples. These measure-
ments were then used to calculate appropriate information density values.

EQUIPMENT

The optical power spectrum measurements were made with a Recording Optical
Spectrum Analyzer (ROSA) manufactured by Recognition Systems, Inc. This
equipment is a general purpose instrument designed for ease and flexibility
of set up. The optical components, all with magnetic mounts, are posi-
tioned on a 72 x 44 inch optical table. A fiberglass shroud covers the
table and components to protect against stray light.

For this study, the equipment is configured generally as shown in Figure 25.
The illumination source is a 7 mw He-Ne laser. Illumination is controlled
with a variable attenuator. The attenuator consists of two opposing glass
wedges that are positioned for the desired transmission level without im-
posing a significant deviation in the laser light path. The laser beam is
expanded with a microscope objective. The magnification of the objective
controls the degree of expansion which, in turn, is determined by the de-
sired area of illumination at the input plane. A 25 mm pinhole is placed
at the focal point of the microscope objective to "clean up" the laser beam.
The laser and microscope objective can be considered as a crude spectrum
analyzer. The pinhole is placed at the Fraunhofer diffraction plane of the
objective and thus passes only the uniform energy in the laser beam. It
acts as a spatial filter that blocks the high frequency variation in the
beam. The expanding beam is then collimated with a lens placed at a dis-
tance from the pinhole equal to its focal length. A 15 inch focal length
telescope objective was used for collimation in this study.

From the collimating lens, the beam passes through the film holder. The
holder is equipped with a variable aperture to control the film area illumi-
nated, circular apertures with diameters from 1/8 inch to 2 and 1/2 inches

TO DATA PROCESSING

AMPLIFIERS AND A/D CONVERTER

SOLID STATE DETECTOR

FILM TRANSPORT

TRANSFORM LENS

P_1: ZERO ORDER DIFFRACTION POINT

P_i: K^{th} ORDER DIFFRACTION BAND

P_1

P_i

APERTURE

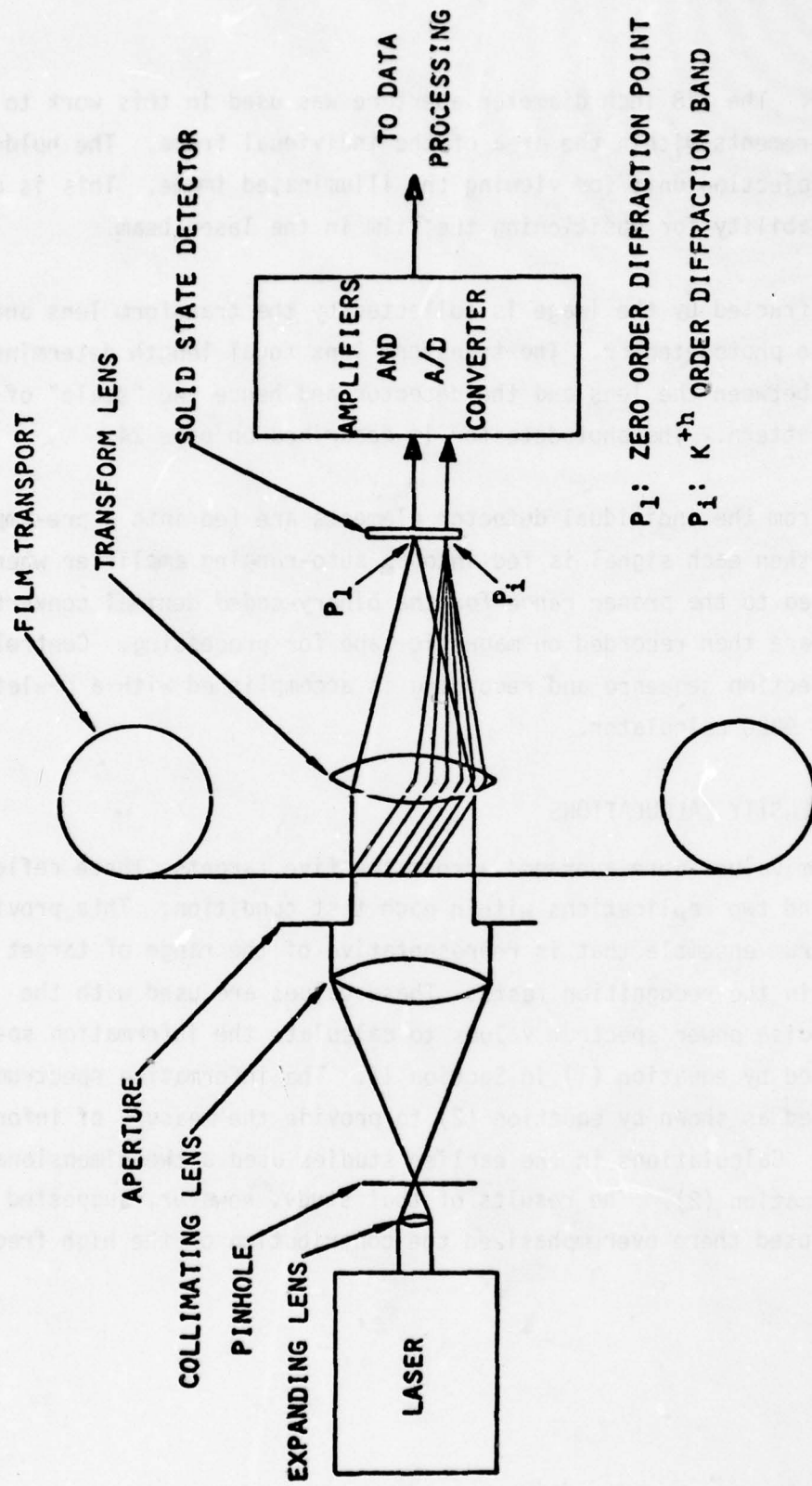COLLIMATING LENS

PINHOLE

EXPANDING LENS

LASER

Figure 25: Recording optical spectrum analyzer.

are available. The 1/8 inch diameter aperture was used in this work to
confine measurements within the area of the individual frame. The holder
includes a projection unit for viewing the illuminated image. This is a
necessary capability for positioning the film in the laser beam.

The light diffracted by the image is collected by the transform lens and
focused on the photodetector. The transform lens focal length determines
the distance between the lens and the detector and hence the "scale" of the
diffraction pattern. The photodetector is described on page 24.

The outputs from the individual detector elements are fed into a pre-amp/
multiplexer, then each signal is fed into an auto-ranging amplifier where
it is converted to the proper range for the binary-coded decimal converter.
These values are then recorded on magnetic tape for processing. Control of
the data collection sequence and recording is accomplished with a Hewlett
Packard Model 9820 calculator.

INFORMATION DENSITY CALCULATIONS

Power spectrum values were averaged across the five targets, three reflect-
ance levels and two replications within each test condition. This provides
a power spectrum ensemble that is representative of the range of target con-
ditions used in the recognition tests. These values are used with the
appropriate noise power spectrum values to calculate the information spec-
trum as defined by equation (1) in Section II. The information spectrum is
then integrated as shown by equation (2) to provide the measure of informa-
tion density. Calculations in the earlier studies used a two-dimensional
version of equation (2). The results of that study, however, suggested that
the approach used there overemphasized the contribution of the high frequency
content.

RESULTS

Information density values for the random bar and dot images are listed in
Table 9. The values are presented in units of bits per degree of visual
angle using the following transformation.

$$V = \frac{r}{2 \tan^{-1}(1/2d)}$$

where   V = frequency in units of cycles per degree,

            r = frequency in units of cycles per millimeter, and

            d = observer's viewing distance (304.8 millimeters
                 in this study).

Although the random dot and bar patterns were not viewed by the observers,
these units are used to permit comparison with the vehicle image measure-
ments.

Table 9: Random Bar and Dot Pattern
Information Density Values (Bits/Degree)

	Baseline	Histogram Equalization	J.N.D. Normalization	Linear Freq. Filter	Logarithms Freq. Filter
Random Bar (vertical)	201.1	207.0	155.2	181.3	185.7
Random Bar (diagonal)	200.3	210.5	156.6	182.8	185.4
Random Bar (horizontal)	204.2	215.0	160.5	184.9	185.8
Random Dot	197.6	217.7	168.6	187.3	190.5

53

Differences among the processing conditions are generally as predicted from theoretical considerations. The histogram equalization process results in the maximum information density. The J.N.D. normalization is less efficient in the formal information sense and shows a relatively greater drop in information density. This is probably due to enhancement of inherent noise using this procedure. The frequency filtering techniques exhibit the expected decline in information density as a result of the low and high frequency filtering. The noise spectra for the two filtering techniques are virtually identical and show only very slight drops below the baseline noise spectra. The evidence indicates that the film grain noise becomes significant at the levels measured and masks the processing noise differences.

Differences among the three orientations of the random bar target indicate that the vertical resolution (horizontal bar orientation) is slightly better than the horizontal resolution. The diagonal bars, as expected, generally provide values between the other two orientations. These orientation effects are constant across processing conditions.

Information density values for the vehicle target ensembles are presented in Table 10.

The major difference in these results from those found for the random bar and dot targets is the decline in information density for the baseline imagery. This is primarily the result of the limited dynamic range in the baseline vehicle imagery compared to the random targets. Since the four processing techniques used contrast stretching, dynamic range differences are essentially eliminated in those cases.

Figure 26 relates the vehicle target information density values to observer performance. The correlation coefficient of -0.33 is not significantly different from zero at the 0.05 probability level.

Table 10: Vehicle Target Information Density
Values (Bits/Degree)

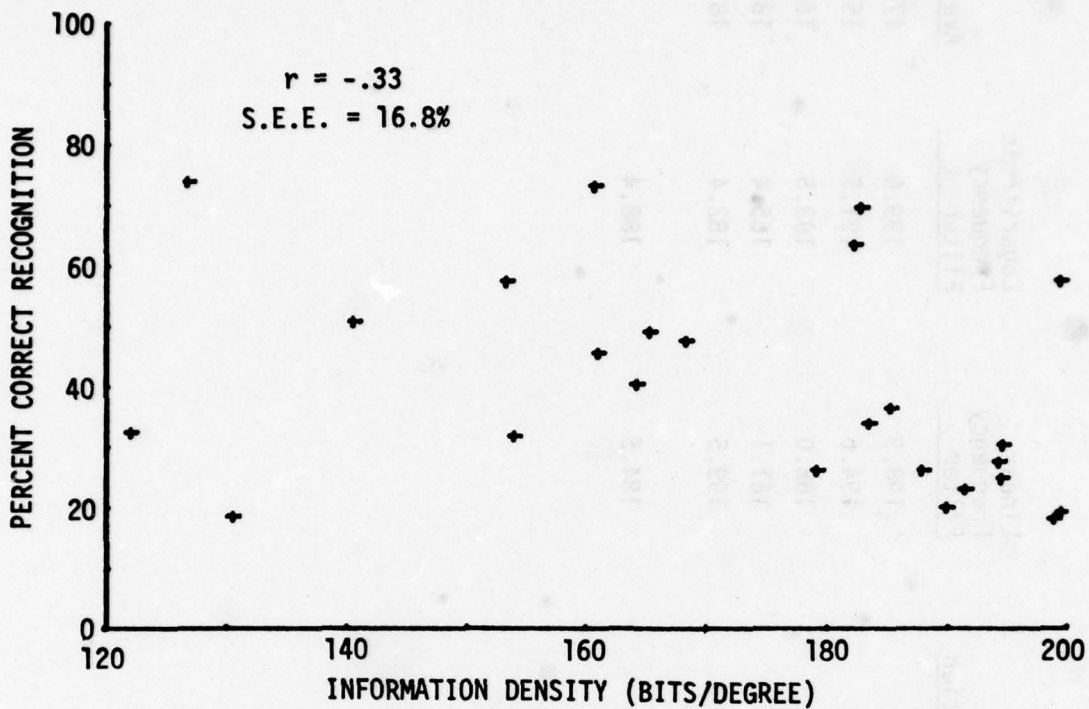| Scale	Baseline	Histogram Equalization	J.N.D. Normalization	Linear Frequency Filter	Logarithmic Frequency Filter	Average
1:4675	130.6	194.3	189.9	198.9	199.6	170.5
1:4110	154.1	194.7	179.2	194.6	191.5	157.8
1:3510	122.2	185.3	164.3	188.0	183.5	168.7
1:2928	140.7	168.4	153.4	161.1	165.4	182.8
1:2363	127.0	182.9	160.8	199.5	182.4	182.7
Average	134.9	185.1	169.5	184.5	188.4	

Figure 26: Performance relationship using information density in units of bits per degree.
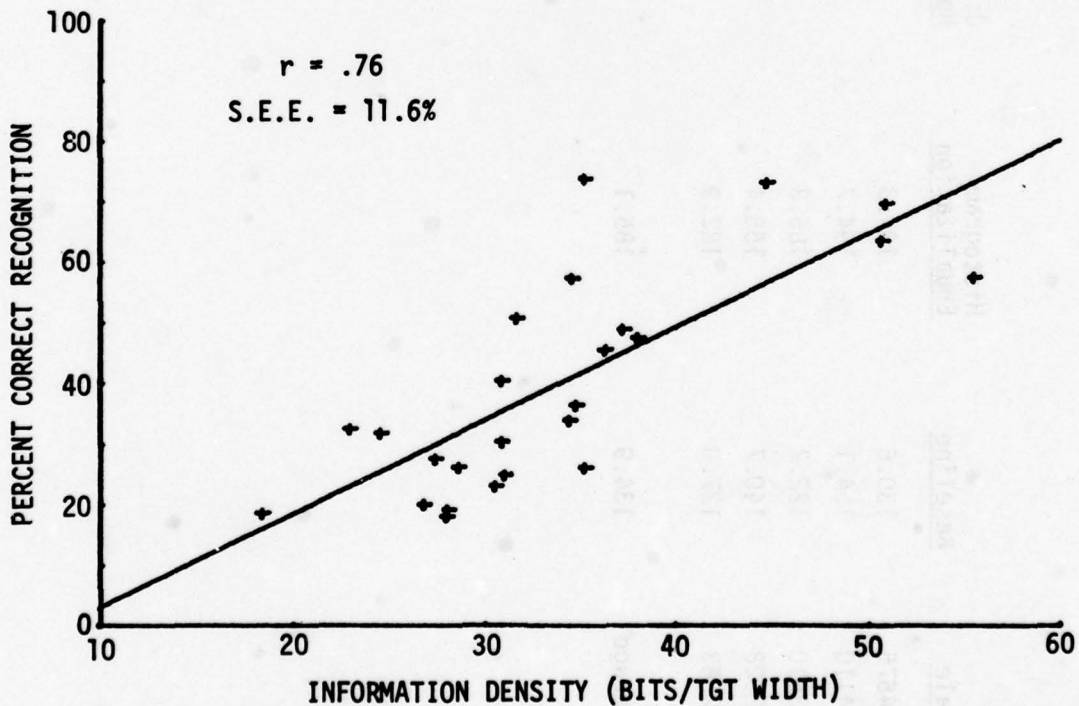

Figure 27: Performance relationship using information density in units of bits per target width.

56

Results of a previous study, Schindler and Martin (1978), indicated significant improvement in performance prediction when corrections for image scale were included. One way to include such a correction is to express information density as a function of target dimensions. Using the transform,

$$t = \frac{r}{w},$$

where,   t = frequency in units of cycles per target width,

                          r = frequency in units of cycles per millimeter, and

                          w = target width in the image (averaged across the five targets),

information density is calculated in units of bits per target width. These values are presented in Table 11. The relationship with performance for information density calculated as bits per target width is shown by the scatterplot in Figure 27. The resulting correlation coefficient of 0.76 represents a significant improvement over the values measured as bits per degree. This value, however, does not represent a satisfactory result since the correlation between performance and scale alone is 0.84. Power spectral data in this situation is detracting from the performance relationship.

Another approach suggested by the results of previous studies is the incorporation of visual threshold data in the information density calculations. Proper implementation of this approach is not likely to be a simple matter. A superficial start was undertaken here to consider the possibility of improvements with consideration of the visual system performance characteristics. The technique applied uses visual sine-wave threshold data (transformed to power units) in place of the image noise power spectrum. It can be shown that for a sine-wave of frequency r,

$$P(r) = .5M_A^2,$$

where

         M_A = the modulation of the sine-wave.

Table 11: Vehicle Target Information Density Values (Bits/Target Width)

Scale	Baseline	Histogram Equalization	J.N.D. Normalization	Linear Frequency Filtering	Logarithmic Frequency Filtering	Average
			Processing Condition			
1:4675	18.4	27.3	26.7	28.0	28.1	25.7
1:4110	24.7	30.9	28.7	31.1	30.7	29.2
1:3510	22.8	34.7	30.8	35.2	34.4	31.6
1:2928	25.0	37.8	34.4	36.2	37.2	34.1
1:2363	35.4	51.0	44.8	55.6	51.8	47.7
Average	25.3	36.3	33.1	36.4	37.2	

As noted earlier, the diffraction pattern sampling technique for estimating the power spectrum is based on the image amplitude distribution. Since most visual threshold values are expressed in terms of intensity modulation, an additional transformation is required. The approximation,

$$M_A \cong .5 M_I$$

where $\qquad M_A$ = amplitude modulation, and

$\qquad\qquad\qquad M_I$ = intensity modulation,

is accurate to ± 1% for values of intensity modulation below 0.2. Under the viewing conditions used in the observer performance tests, the maximum frequency of interest in the imagery (Nyquist limit) is about 27 cycles per degree. The threshold values used in this study do not reach a value of 0.2 over this frequency range. The transformation used then is

$$P(r) = .125 \, M_I^2 \, .$$

The threshold data used is taken from the curve reported by Farrell and Booth (1975). This curve, shown in Figure 28, is a composite of results from nine individual studies. The transformed power threshold curve is shown in Figure 29.

The values from Figure 29 were substituted for noise power to calculate information density. Equation (1) in Section II thus becomes,

$$D(k) = Log_2 \frac{P_{m+s}(k)}{P_t(k)} \, ,$$

where $\qquad D(k)$ = information content (bits/cycle) at frequency (k),

$\qquad\qquad\qquad P_{m+s}(k)$ = relative power at frequency k for the image of interest, and

$\qquad\qquad\qquad P_t(k)$ = relative power for visual threshold sine wave at frequency k.

$$M_A = \frac{1}{2} M_I$$

where M_A = amplitude modulation, and

          M_I = intensity modulation.

is accurate to ± 1% for values of intensity modulation below 0.2. Under the viewing conditions used in the observer performance tests, the highest frequency of interest in the imagery (Nyquist limit) is about 27 cycles per degree. The threshold values used in this study do not reach a value of 0.2 over this frequency range. The transformation used then is

Figure 28: Visual sine-wave threshold curve.

The threshold data used is taken from the curve reported by Carrell and Booth [1-25]. This curve, shown in Figure 28, is a composite of results from nine individual studies. The transformed power threshold curve is shown in Figure 29.

The values from Figure 29 were substituted for noise power to calculate information density. Equation (11) in Section II thus becomes,

$$D(f) = \log \frac{P_{in}(f)}{P_t(f)}$$

where $D(f)$ = information density (bits/cycle) at frequency f,

          $P_{in}(f)$ = relative power at frequency f (for the image of interest), and

          $P_t(f)$ = relative power for visual threshold sine wave at frequency f.
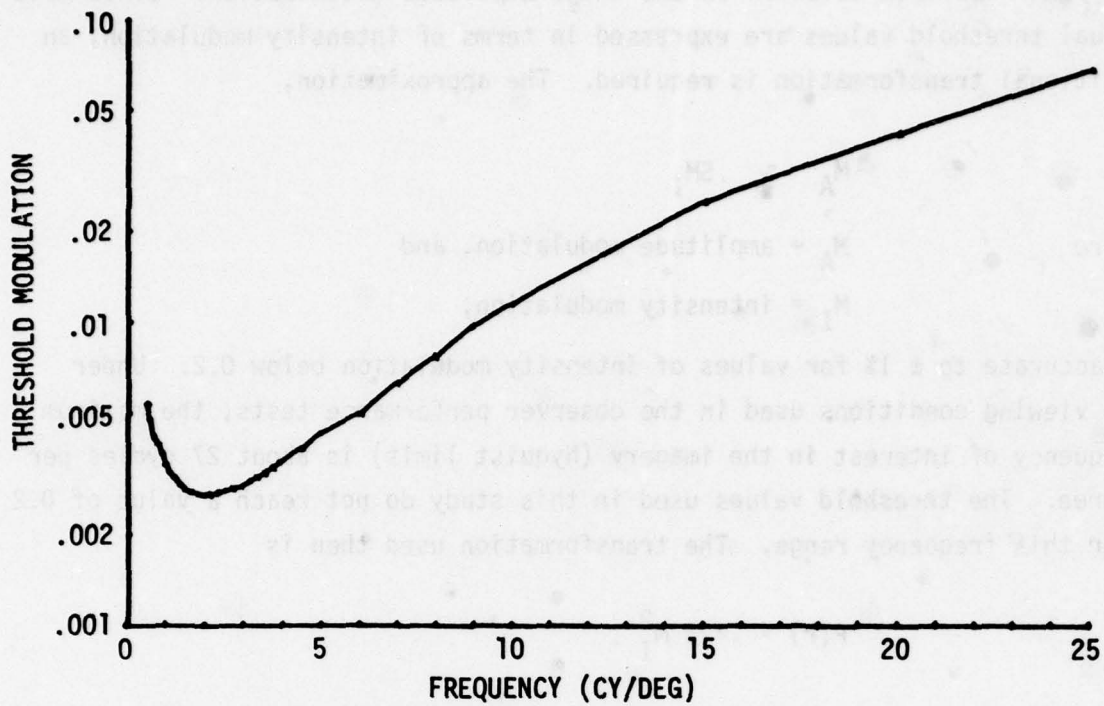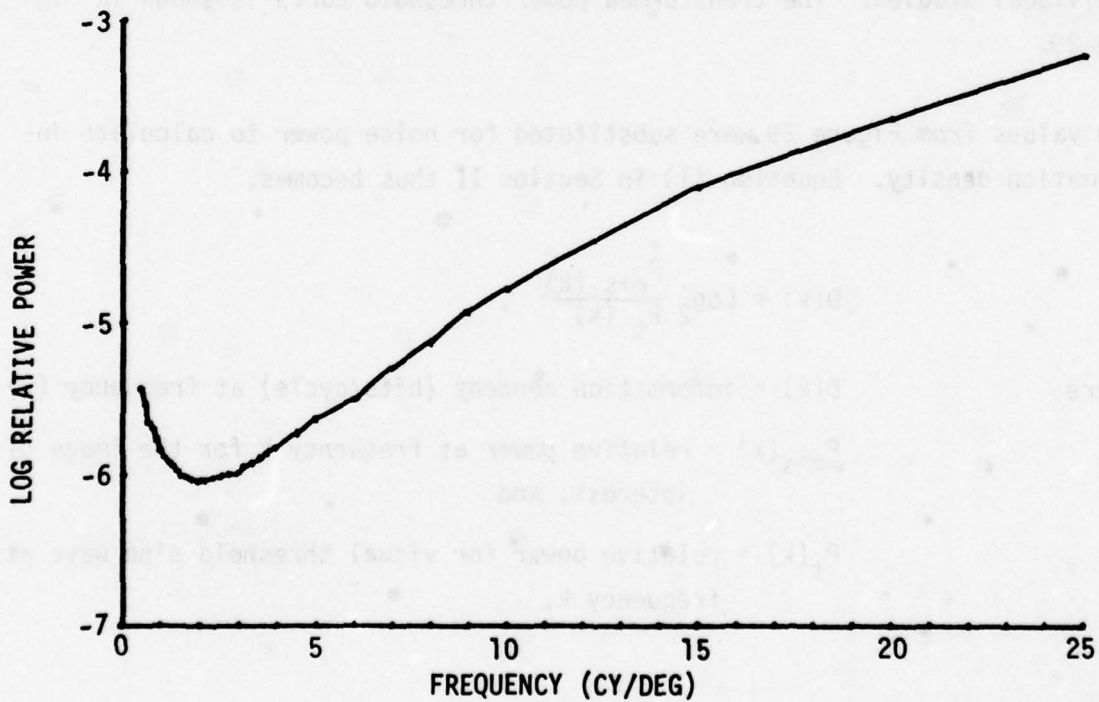

Figure 29: Threshold values transformed to units of relative power.

60

The resulting values are integrated and transformed to units of bits per target width as in the previous calculations. The results are presented in Table 12. The scatter plot relating these information density values to performance scores is shown in Figure 30. The correlation coefficient of 0.87 is a significant improvement over the previous results but an obvious problem remains. The circled data points are the baseline image results and they are consistently discrepent relative to the information density values associated with the various processes. For a given level of performance, the measured information density values are consistently lower for the baseline imagery than for any of the processed imagery. As a result, the information density values improperly rate the baseline condition as the poorest (see Table 12). As noted earlier, the power spectral values tend to be overly sensitive to overall image contrast levels. A correction for this effect appears to be a desirable consideration.

As discussed by Nill (1976), a measure of overall image contrast is provided by total normalized, non-zero frequency power.

$$C = \frac{\sum\limits_{k=0}^{K} \left[P(k) - P(0) \right]}{\sum\limits_{k=0}^{K} P(k)} \tag{3}$$

where

$P(k)$ = power at frequency k, and
K = maximum useful frequency.

The equation above was used to calculate overall contrast values for each image. These values were averaged across target type and reflectance level and used in a multiple regression analysis along with information density (corrected for threshold) to determine a best fit equation with performance scores. The best relationship was found to occur with the logarithm of overall contrast. The resulting regression coefficient for overall contrast (- 29.4 log C) is incorporated in the scatter plot shown in Figure 31. This fit provides a correlation coefficient of 0.95 and represents an excellent relationship with observer performance scores. The individual values are presented in Table 13.

61

Table 12: Vehicle Target Information Density Values with
Visual Threshold Corrections (Bits/Target Width)

Processing Condition

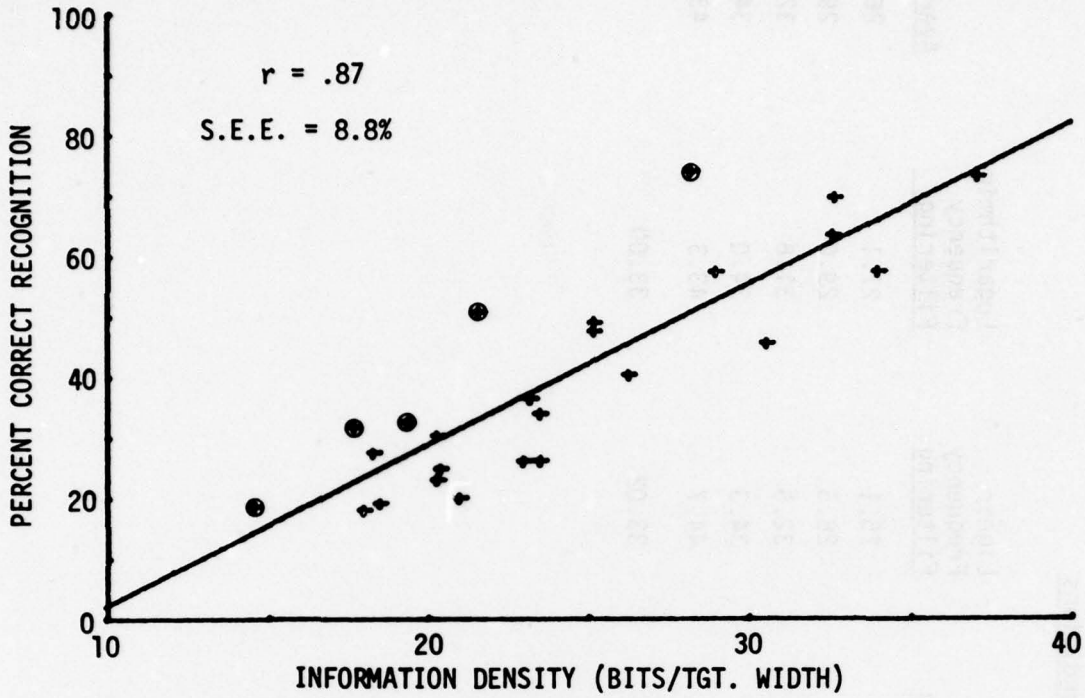| Scale	Baseline	Histogram Equalization	J.N.D. Normalization	Linear Frequency Filtering	Logarithmic Frequency Filtering	Average
1:4675	14.6	18.3	21.0	17.9	18.5	18.1
1:4110	17.3	20.3	23.1	20.4	20.4	20.4
1:3510	19.3	23.2	26.2	23.4	23.4	23.1
1:2829	21.6	25.1	28.8	24.6	25.1	25.0
1:2363	28.4	32.7	37.2	34.0	32.6	33.0
Average	20.3	23.9	27.3	24.0	24.1	

Figure 30: Performance relationships using information density with visual threshold correction.
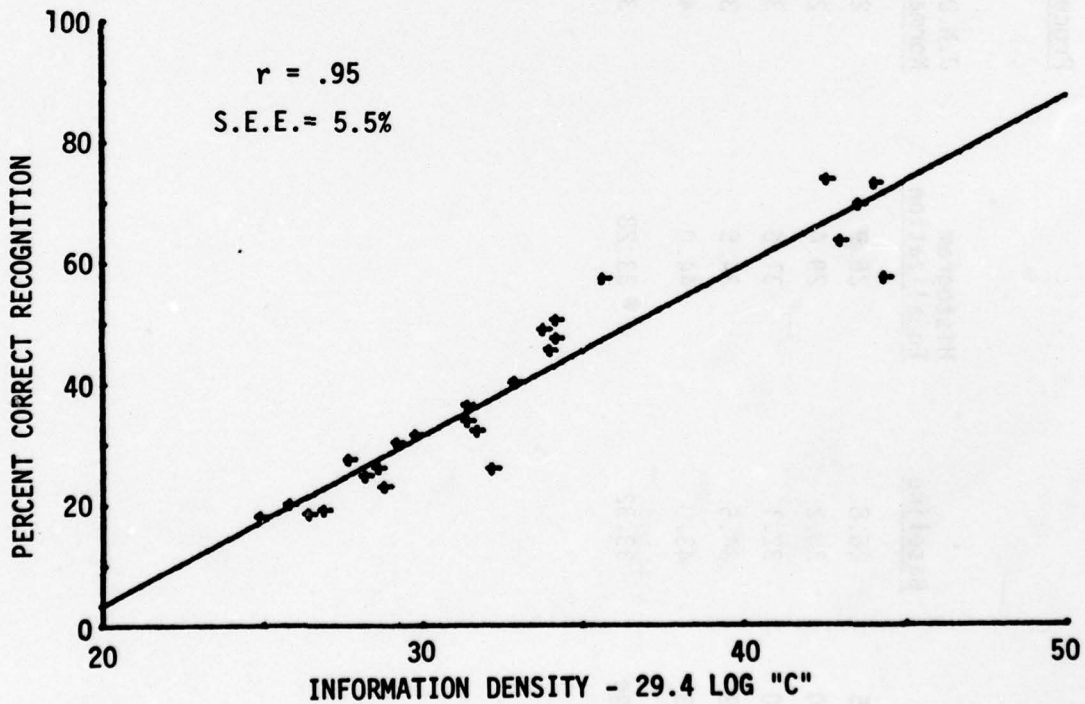
Figure 31: Performance relationships using information density with threshold and overall contrast corrections.

Table 13: Information Density Values with Visual Threshold and Contrast Corrections

Processing Conditions

Scale	Baseline	Histogram Equalization	J.N.D. Normalization	Linear Frequency Filtering	Logarithmic Frequency Filtering	Average
1:4675	26.8	26.9	26.0	25.1	27.1	26.4
1:4110	30.2	29.4	28.7	28.5	29.0	29.2
1:3510	32.1	31.6	33.1	32.5	31.6	32.2
1:2928	34.5	34.5	35.9	34.3	34.0	34.6
1:2363	43.0	44.0	44.3	44.7	43.3	43.9
Average	33.32	33.28	33.60	33.02	33.00	

64

SECTION VII
METHODOLOGY FOR PROCESSING TECHNIQUE SELECTION

A major problem in the practical application of digital image processing
is the selection of the best processing technique for a specific image.
Experience has shown that no single technique is best for all images.
The observer performance results in Section V demonstrate similar con-
clusions (for example, see Figure 24, page 49). As a result of this prob-
lem, most digital processing is performed on a "try and see" basis. The
operator selects the most promising techniques from those available to
him and observes the results until he is satisfied that the best image
has been produced. This is a very time consuming method and relies heavily
on the judgement and experience of the operator.

The general methodology developed in Section VI appears promising for the
quantitative evaluation of processing results but it is of limited utility
for the selection problem because it does not permit a decision before
first processing the image. An acceptable method is one that allows a
selection decision based on the characteristics of the original image be-
fore any processing is performed.

The results in Section VI suggest that overall contrast and information density
with threshold correction are effective descriptors of the digitized imagery
used in this study. If these characteristics of the original imagery could
be used to predict performance after processing, then such predictions could
be used to select the processing technique, if any, likely to be the most
effective. Such a method was implemented in this study. Multiple regression
was used to develop five prediction equations, one for each processing con-
dition, including the baseline imagery. These equations use log overall con-
trast and information density for the original (base line) images to predict
performance separately for each processing condition.

The results presented in Section VI are based on power spectrum ensembles of
target types and reflectance levels. Although this is a more realistic approach
(targets and their reflectance levels will vary in any practical situation), it
seriously reduces the number of data points for the development and validation

65

of the prediction equations. In order to maximize the stability of the quations, all of the data used were separated by reflectance level as well as scale and processing condition. This provides 15 sets of data points for each equation. The equations relate information density (with visual threshold correction) and overall contrast as defined by equation (3) with observer performance for each of the processing conditions. The equations are of the form;

$$\hat{p} = K + LD_c + M \log C,$$

where,

$\hat{p}$ = predicted observer performance level,

K, L, M = regression coefficients,

D_c = information density with threshold correction, and

C = overall contrast.

Table 14 presents the resulting equations and correlation coefficients.

The equations in Table 14 can be used to plot a "decision space" as shown in Figure 32. This figure shows three areas of maximum performance for the conditions tested in this study. The two frequency filtering techniques are not represented since they did not yield maximum performance for any image. The graph is limited to the range of values tested in this study. Such a graph might be used in the following manner:

1) Contrast and information density are measured on an original image of interest.

2) The intersection of the measured values indicates the processing technique, if any, that is likely to provide the best performance.

It must be noted that the values presented in this section are primarily to illustrate a suggested methodology. The scope of this study both in terms of image characteristics and processing techniques is too limited to warrant the actual application of these data.

66

Table 14: Calibration Equations for Process Selection

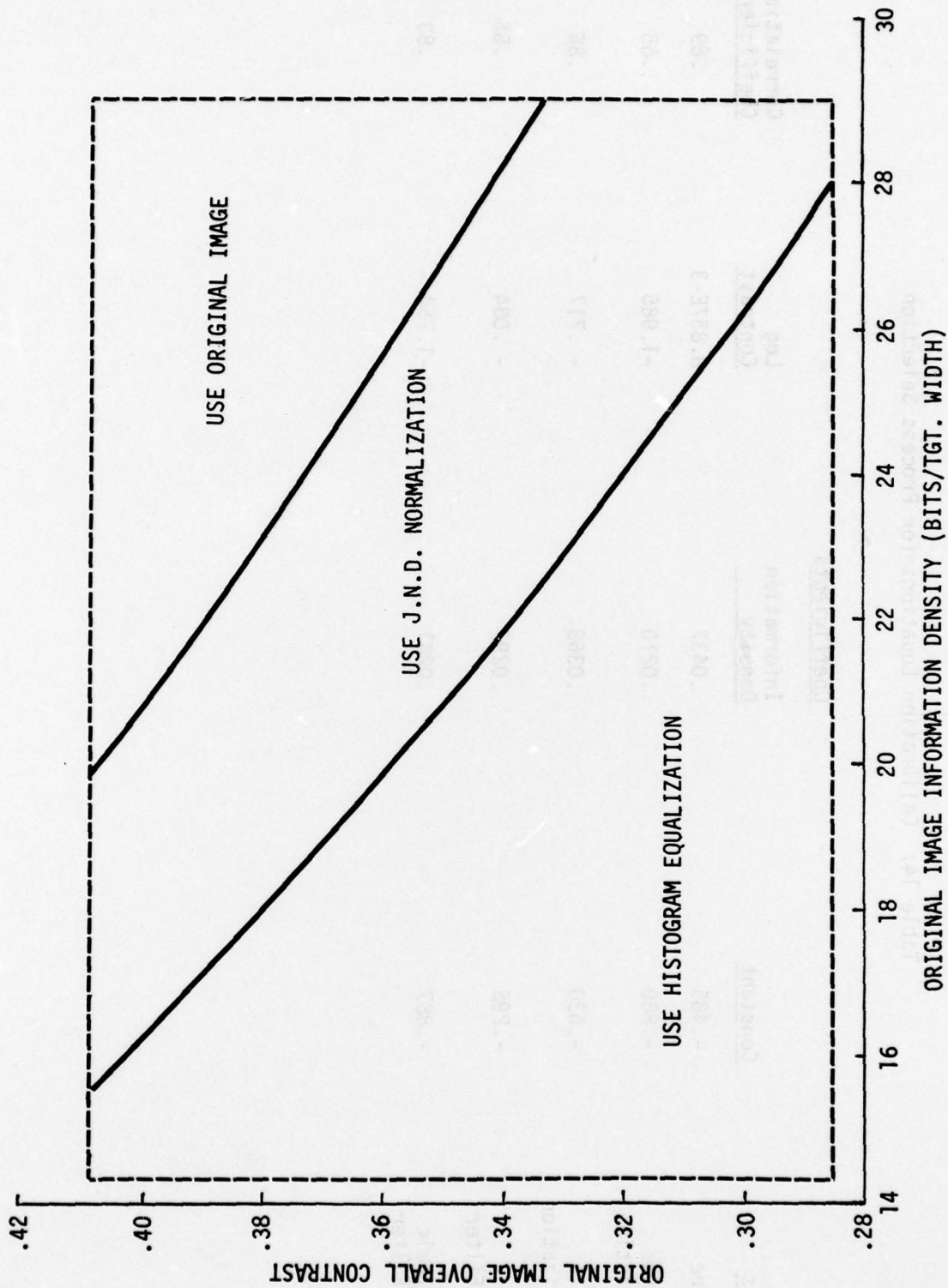| Process	Constant	Coefficients		Correlation Coefficient
		Information Density	Log Contrast	
Baseline	-.485	.0437	8.837E-3	.89
Histogram Equalization	-.880	.0210	-1.985	.85
J.N.D. Normalization	-.630	.0368	-.717	.86
Linear Freq. Filter	-.295	.0297	-.084	.85
Logarithmic Freq. Filter	-.887	.0241	-1.754	.83

Figure 32: Decision space for selection of processing technique.

Although this approach to processing selection reduces the time and effort
from that required for the "try and see" approach, it still requires print-
ing of the original image. Since the image data is already in digital form,
it is possible to calculate the power spectrum and information density val-
ues directly. This was done for each of the base-line images as a part of
the original processing using a Fast Fourier Transform routine with the
Interdata computer. The modulation transfer function for the laser beam
recorder (Figure 18) was incorporated in the power spectral calculations.
This was done so that resulting values would be representative of conditions
in the actual print.

Thus, $\qquad P(k)_d = P(k) \; [MTF(k)]^2$,

$\qquad P(d)_d$ = the corrected power value for frequency k,

$\qquad P(k)$ = the calculated power value for frequency k, and

$\qquad MTF(k)$ = the laser beam recorder modulation transfer
$\qquad\qquad\qquad\quad$ factor for frequency, k.

Normally, these calculations should include a correction for the printing
gamma. However, since a gamma of unity was used for printing in this study,
such a correction was not required. The resulting power spectra were aver-
aged across target types. This provided an ensemble of 5 spectra for informa-
tion density calculations. Information density values with visual threshold
corrections were determined in the same manner as with the optical data. Over-
all contrast values were similarly calculated.

Figure 33 provides a plot of the relationship between the optically and digi-
tally derived information density values. The resulting correlation coeffi-
cient of 0.95 indicates good promise for the digital approach. In order to
assess the selection effectiveness of both the optical and digital approaches,
all values were averaged across reflectance levels and decision values calcu-
lated with the coefficients shown in Table 14. New equations to fit the

69
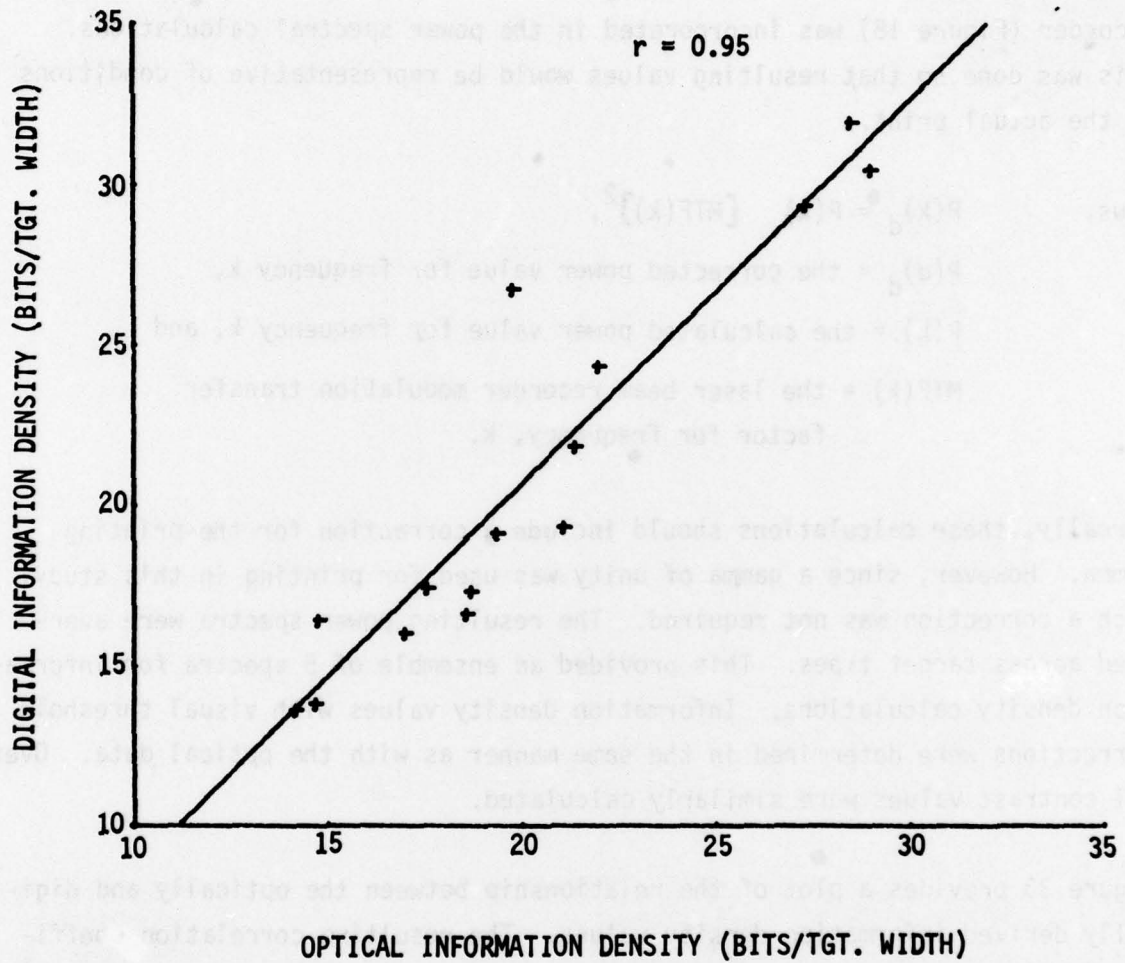
Figure 33: Correlation between optically and digitally derived information density values.

digital data were not developed. The resulting values are presented in Table 15 along with observer performance scores. The specific selections are summarized in Table 16 and compared with the techniques providing the best performance.

The effectiveness of this approach cannot be properly evaluated because of the limited sample of imagery and processing techniques used here. Where errors were made, both selection approaches picked the second best process and in all cases the performance difference was very small. These results, however, are likely to be over optimistic since for the optical selection, at least, the decision equations were fitted to the data. A proper evaluation will require an independent set of data for purposes of validation. The digital data are also contaminated because the same imagery and performance scores were used. The primary intention of this exercise is to illustrate the application of these techniques and demonstrate their feasibility.

Table 15: Processing Selection Decision Values

Scale		Baseline	Histogram Equalization	J.N.D. Normalization	Linear Freq. Filter	Logarithmic Freq. Filter
				Processing Condition		
1:4675	Perf.	.18	.28	.20	.18	.19
	Optical	.15	.25	.20	.17	.19
	Digital	.15	.29	.22	.22	.18
1:4110	Perf.	.32	.30	.26	.25	.23
	Optical	.29	.33	.32	.27	.28
	Digital	.24	.33	.30	.28	.24
1:3510	Perf.	.32	.36	.40	.26	.34
	Optical	.35	.29	.29	.31	.34
	Digital	.43	.43	.46	.37	.39
1:2928	Perf.	.50	.48	.57	.46	.49
	Optical	.45	.44	.48	.38	.40
	Digital	.46	.46	.49	.41	.39
1:2363	Perf.	.74	.70	.77	.59	.67
	Optical	.75	.70	.77	.59	.65
	Digital	.85	.66	.82	.64	.65

Table 16: Selection Summary

Scale	Best Performance	Optical Selection	Digital Selection
1:4675	Histo. Equal.	Histo. Equal.	Histo. Equal.
1:4110	Base-line	Histo. Equal.	Histo. Equal.
1:3510	J.N.D.	Histo. Equal. or J.N.D.	J.N.D.
1:2928	J.N.D.	J.N.D.	J.N.D.
1:2363	Base-line	J.N.D.	Base-line

SECTION VIII
CONCLUSIONS

It is important to recognize several limitations on the data when inter-
preting the results of this study. The digital processing techniques
were selected as representative not as optimum. They were implemented
in a standard routine manner with no attempt to "touch up" or modify the
results. The imagery was limited in scope. The background was identical
in all images and the five target vehicles were well known to the ob-
servers. Caution is necessary in interpreting the results of the observer
performance tests because of the strong interactions with scale and re-
flectance level, and because of the small overall processing condition
differences.

Under the conditions tested here:

1) The histogram modification techniques (histogram equalization
   and J.N.D. normalization) were the most successful, particu-
   larly with low contrast imagery.

2) All processing techniques performed poorly with high reflectance
   targets, probably because of saturation with the contrast stretch-
   ing.

3) Both frequency filtering techniques performed poorly although
   the "homomorphic" (logarithmic) technique was clearly superior
   to the linear model.

4) The "pure" theoretical information density measure is not
   effective as a measure of processing effects on observer per-
   formance ($r = -.33$).

5) Corrections for visual sine-wave thresholds and for overall
   image contrast greatly improve the information density re-
   lationships with performance ($r = .95$).

6) A process selection technique based on modified information
   density measures of the original (base-line) image is a feasible
   alternative to the "try and see" approach to digital image pro-
   cessing. Measures calculated directly from the original digital
   data may also be used for this purpose.

74

REFERENCES

1. Agrawal, J. P., and O'Neal, J. B. Jr., "Low Bit Rate Differential PCM for Monochrome Television Signals". *IEEE Trans. Communications*, Vol. COM-21, No. 6, pp. 706-714, 1973.

2. Andrews, H. C., "Monochrome Digital Image Enhancement", *Applied Optics*, Vol. 15, No. 2, pp. 495-503, 1976.

3. Dainty, J. C., and Shaw, R., *Image Science - Principles, Analysis and Evaluation of Photographic Type Imaging Processes*, Academic Press, New York, 1974.

4. Ditchburn, R. W., *Light*, 2nd Edition, Interscience Publishers, 1963.

5. Farrell, R. J., and Booth, J. M., *Design Handbook for Imagery Interpretation Equipment*, Boeing Aerospace Company Report D180-19063-1, Seattle, Washington, 1975.

6. Gaven, J. V., Tavitian, J., and Harabedian, A., "The Informative Value of Sampled Images as a Function of the Number of Gray Levels Used in Encoding the Images", *Photographic Science and Engineering*, Vol. 14, pp. 16-20, 1970.

7. Gonzalez, R. C., and Wintz, P., *Digital Image Processing*, Addison-Wesley Publishing Company, Reading, Mass., 1977.

8. Goodman, J. W., *Introduction to Fourier Optics*, McGraw-Hill Book Co., New York, 1968.

9. Guilford, J. P., *Psychometric Methods*, McGraw Hill, New York, N. Y., 1954.

10. Hall, E. L., "Almost Uniform Distributions for Computer Image Enhancement", *IEEE Transactions on Computers*, Vol. VC-23, pp. 207-208, 1974.

11. Humes, J. M., and Bauerschmidt, D. K., *Low Light Level T.V. Viewfinder Simulation Program, Phase B, The Effects of Television System Characteristics Upon Operator Target Recognition Performance*. Report AFL-TR-68-271, Air Force Avionics Laboratory, Wright-Patterson Air Force Base, Ohio, 1968.

12. Hunt, B. R., "Computers and Images", in <u>Image Processing Proceedings</u> <u>of the Seminar, Pacific Grove, Calif., February 24-26, 1976</u>, Soc. of Photo-Optical Instrumentation Engineers, pp. 3-9, 1976.

13. Jensen, N., High Speed Image Analysis Technique, <u>Photogrammetric Eng.</u>, Vol. 39, pp. 1321-1328, 1973.

14. Kasdan, H. L., Optical Power Spectrum Sampling and Algorithms, <u>Proc.</u> <u>Soc. Photo-Optical Instr. Eng.</u>, Vol. 117, pp. 67-74, 1977.

15. Ketcham, D. J., Lowe, R. W., and Weber, J. W., <u>Image Enhancement Tech-</u> <u>niques for Cockpit Displays</u>, Report ONR-CR213-124-2, Office of Naval Research, Arlington, Virginia, 1976.

16. Leachtenauer, J. C., Optical Power Spectrum Analysis: Scale and Reso- lution Effects, <u>Photogrammetric Eng., & Remote Sensing</u>, Vol. 43, No. 9, pp. 1117-1125, 1977.

17. Lendaris, G. C., and Stanley, G. L., Diffraction Pattern Sampling for Automatic Pattern Recognition, <u>Proc. of IEEE</u>, Vol. 58, No. 2, pp. 198- 216, 1970.

18. Lukes, G. E., Rapid Screening of Aerial Photography by OPS Analysis, <u>Proc. Soc. Photo-Optical Instr. Eng.</u>, Vol. 117, pp. 89-97, 1977.

19. Mannos, J. L., and Sakrison, D. J., "The Effects of a Visual Fidelity Criterion on the Encoding of Images", <u>IEEE Trans. on Information Theory</u>, Vol. 1T-20, pp. 525-536, 1974.

20. Nill, N., The Moment as an Image Quality Merit Factor for Scene Power Spectra, <u>Applied Optics</u>, Vol. 15, p. 2846, 1976.

21. Pratt, W. K., <u>Digital Image Processing</u>, John Wiley & Sons, New York, N. Y., pp. 314-316, 1978.

22. Rogers, J. G., and Carel, W. L., <u>Development of Design Criteria for Sen-</u> <u>sor Displays</u>, Hughes Aircraft Company Report No. C 6619, Culver City, Calif., 1973.

23. Rosenfeld, A., and Kak, A. C., <u>Digital Picture Processing</u>, Academic Press, New York, N. Y., 1976.

24. Schindler, R. A., and Martin, W. L., <u>Optical Power Spectrum Analysis of Display Imagery</u>, Report AMRL-TR-78-50, Aerospace Medical Research Laboratory, Wright-Patterson Air Force Base, Ohio, 1978.

25. Shannon, C. E., and Weaver, W., <u>The Mathematical Theory of Communication</u>, University of Illinois Press, Urbana, Ill., 1949.

26. Smith, F. G., and Thompson, J. H., <u>Optics</u>, John Wiley & Sons Ltd., New York, 1971.

27. Stockham, T. G., Jr., "Image Processing in the Context of a Visual Model", <u>Proc. IEEE</u>, Vol. 60, pp. 828-842, 1972.

28. University of Southern California, <u>Bibliography on Digital Image Processing and Related Topics</u>, U.S.C. Dept. of Electrical Engineering Report No. 410, 1972.